Numerical Modeling of Single Shell Roofs

Késio Palácio, Paulo B. Lourenço, Joaquim Barros

Report 03-DEC/E-21

The present research has been carried out under
contract GROW-1999-70420 "ISO-BRICK" from the European Commission
Task 1.2

Date: August 2003
No. of Pages: 42

Keywords: finite-element method, reinforced masonry shells, structural analysis

Escola de
Engenharia

Departamento de
Engenharia Civil

Universidade
do Minho

Azurém, 4800-085 Guimarães - Tel. +351 253 510 200 - Fax +351 253 510 217 - E-mail secG@civil.uminho.pt

Contents

1 Introduction 3

2 Description of the Non-Linear Material Model 5

2.1 Adopted finite elements 5

2.2 Constitutive models 8

3 Analysis of Reinforced Masonry Shells 19

4 Conclusions 33

5 References 34

ANNEX A 36

A.1 Mechanical properties for mortar 37

A.2 Mechanical properties for Layer 1 - Mortar 38

A.3 Mechanical properties for Layer 2 - Masonry 39

A.4 Mechanical properties for the steel 41

Azurém, P – 4800-058 Guimarães Tel. +351 253 510200 • Fax +351 253 510217

1 Introduction

Shell surfaces provide a structurally efficient solution to the problem of carrying roof loads over long spans. These three-dimensional forms owe their efficiency to the translation of applied loads into tensile and compressive stress, as well as shear stress, in the plane of their surface. These are termed membrane stresses. Shells may be single curved in one direction, e.g. in the form of cylinder, or double curved, e.g. to form a dome or a saddle-shaped surface, see *Figure 1.1*.

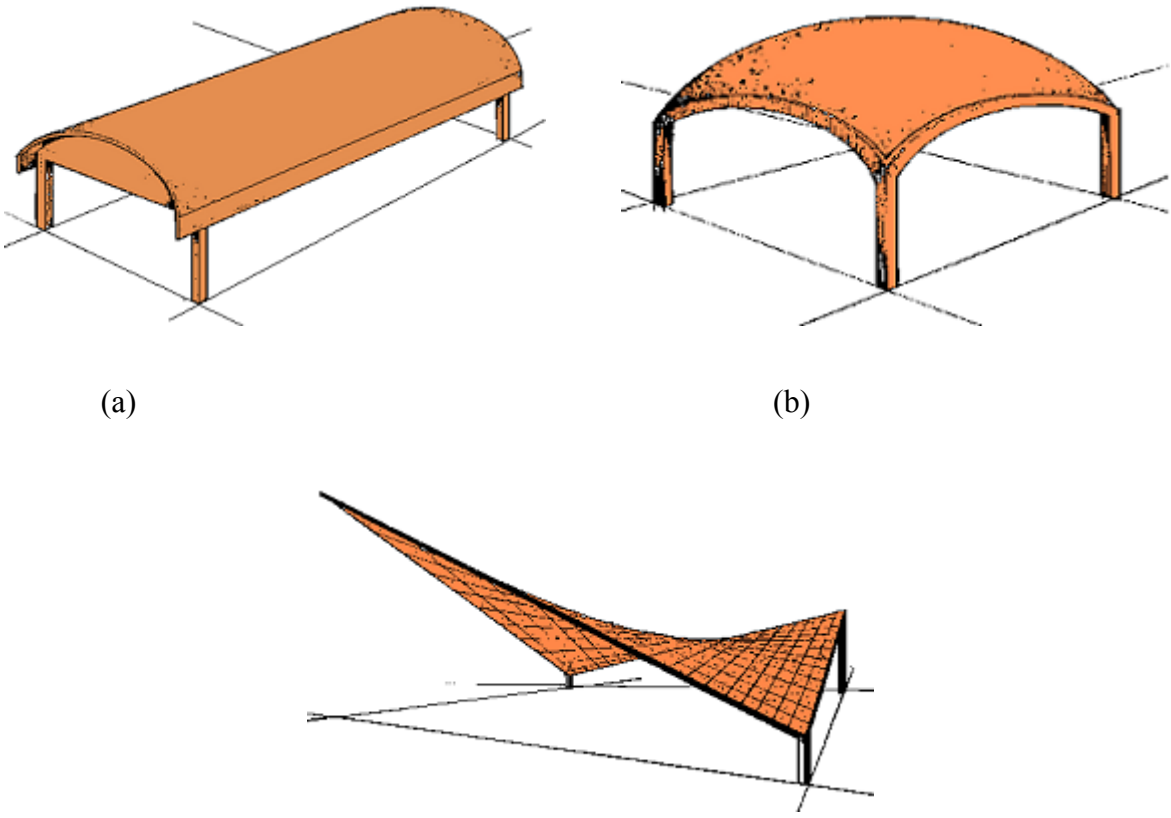

(a) (b)

(c)

Figure 1.1– Examples of shell roofs: a) barrel vault; b) dome; c) saddle dome

There is a significant amount of literature on the analysis of shell structures, covering linear elastic, plastic, stability and collapse analyses. Shell structures are by

Azurém, P – 4800-058 Guimarães Tel. +351 253 510200 • Fax +351 253 510217

nature complex, and the mathematics involved in a shell analysis exhibit large difficulties. Therefore, a valuable tool to assess the structural response of shell structures is the finite element method (FEM). In addition to the possibility to accommodate any boundary condition and form of loading, shell finite-elements can also be subdivided into layers, allowing the structural simulation of shell surfaces with different materials.

Many constitutive models have been developed in the scope of the finite element method to evaluate the nonlinear behavior of many construction materials, especially concrete and metals. In the case of masonry, there are very few models that have been developed, e.g. by Dhanasekar et al. (1985), Lourenço et al. (1998) and Berto et al. (2002). However, smeared cracking models, which are material models for isotropic brittle/quasi-brittle materials implemented in most advanced finite element programs, may be used, under specific circumstances, to describe the non-linear behavior of masonry. In this work, given the uniaxial behavior of the tested masonry shells, the isotropic smeared cracking model has been selected due to its simplicity and wide availability.

It is noted that very few publications address the analysis or design of reinforced masonry shells, as the ones adopted here. Thus, besides the discussion of the experimental results in light of the results of the numerical analysis, this report also addresses a sensitivity study, in order to define the analysis parameters that play important roles in the behavior of these structures.

Azurém, P – 4800-058 Guimarães Tel. +351 253 510200 • Fax +351 253 510217

2 Description of the Non-Linear Material Model

The present work addresses modeling of laminar masonry structures (plates and shells), which can adequately be represented by plane stress conditions. Here, the adopted plane stress element and possible shell finite element to adopt in double curvature shells are briefly introduced, together with the adopted non-linear materials models that are usually available in non-linear finite element packages.

2.1 Adopted finite elements

For plane stress analysis, the eight-noded finite element, with quadratic interpolation of the displacement field, was adopted. *Figure 2.1* illustrates the isoparametric element adopted.

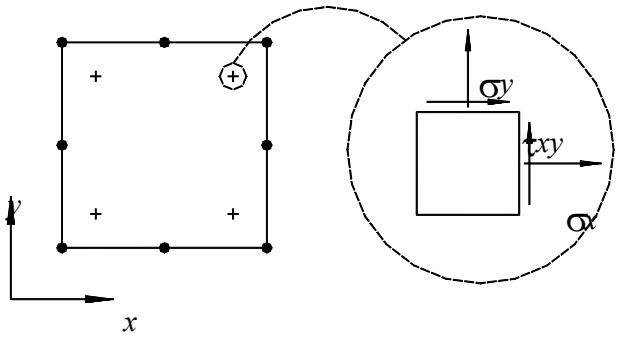

Figure 2.1- Plane stress element

For possible applications in double curvature shells, it is stressed that plates and shells are a particular form of a three-dimensional solid, whose mathematical treatment presents no theoretical difficulties. Owing to the symmetry of the stress and strain tensors, it is normal to collect the tensors components, see *Figure 2.2*, in vectors as

Azurém, P – 4800-058 Guimarães Tel. +351 253 510200 • Fax +351 253 510217

$$\begin{cases} \{\sigma\} = \{\sigma_x, \sigma_y, \sigma_z, \tau_{xy}, \tau_{yz}, \tau_{xz}\}^T \\ \{\varepsilon\} = \{\varepsilon_x, \varepsilon_y, \varepsilon_z, \gamma_{xy}, \gamma_{yz}, \gamma_{xz}\}^T \end{cases} \tag{2.1}$$

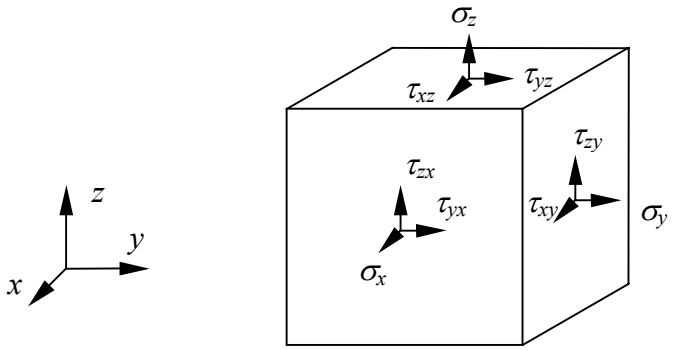

Figure 2.2- Stress components in a three-dimensional body

However, the thickness of plates and shells (denoted as *t*) is small when compared with other dimensions, and complete three-dimensional numerical treatment would be, in general, not only costly but in addition could lead to serious equation conditioning problems. Here, no discussion is given regarding the approximations involved or the range of validity of the theories.

The curved shell element reduce the degrees-of-freedom in a complete three-dimensional analysis, which is an element degenerated from a three-dimensional formulation. This element has been extensively used for the geometrical and material non-linear analysis of shell structures. Typical characteristics of this element are the two hypotheses on which the degeneration is based: "straight normals" and "zero normal stress". The first hypothesis assumes that the normals to the mid-plane of the element remain straight after deformation, but not necessarily perpendicular to the mid-plane. The second hypothesis, already introduced above, states that the normal stress component perpendicular to the mid-plane equals zero, and the element formulation has been obtained ignoring the strain energy resulting from this stress. Assuming that the local z-axis represents the normal to the mid-plane, the five stress components left are σ_x, σ_y, τ_{xy}, τ_{yz} and τ_{xz}, see *Figure 2.3*.

Azurém, P – 4800-058 Guimarães Tel. +351 253 510200 • Fax +351 253 510217

Five degrees of freedom are defined for each element node: three translations and two rotations, see *Figure 2.4*. The definition of the independent translations and rotations includes the influence of shear deformation. The rotations are not coupled to the gradient of the mid-plane. Besides, as was said before, the thickness of shell finite elements can be subdivided in layers, allowing different layer materials to be inserted in unique element. For practical applications, two by two Gauss integration in the plane and seven-point Simpson integration in the thickness direction are recommended.

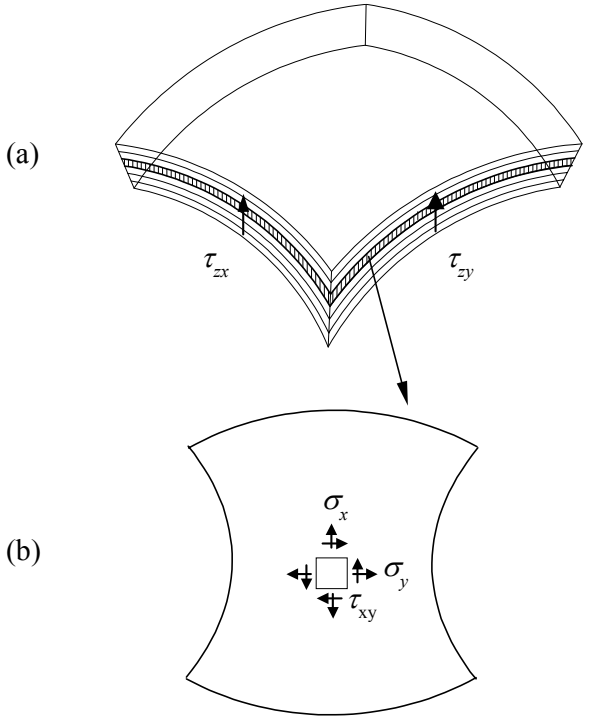

Figure 2.3- Thin shells: (a) layered shell with five stress components; (b) layer, essentially, in plane stress conditions

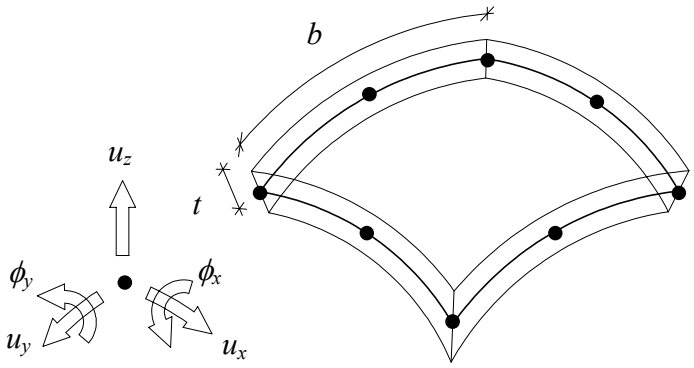

Figure 2.4- Curved shell element (applicable for thin shells with t << b)

Azurém, P – 4800-058 Guimarães Tel. +351 253 510200 • Fax +351 253 510217

2.2 Constitutive models

The main cause of the non-linearity of quasi-brittle materials is cracking, which is due to the limited capacity of these materials to sustain tensile stress. Currently, in the DIANA Finite Element Package, TNO (2003), adopted for the analysis there are two basic material models for modeling cracking in brittle materials, which are the so-called smeared cracking models, after Rashid (1968), and crack models based on total strain, after Vecchio and Collins(1986). The latter model is a complete one, describing tensile behavior as well as compressive behavior whereas the former adopts a combination of a plasticity model, to describe the compressive behavior, and a cracking model. Both models are briefly reviewed next. For simplicity, smeared crack models with combination of plasticity models will be termed here as Elasto-Plastic-Cracking models.

2.1.1 Elasto-Plastic-Cracking model

This commonly used material model for concrete-like materials combines a smeared cracking model for tension with a plasticity model for compression:

- Compressive behavior – plasticity model

In multi-axial stress states the compressive stress can exceed the compressive strength of the material. In this case the crack model can be combined with a plasticity model that describes the crushing of the material. This plasticity model is based on the flow theory of plasticity, where the nonlinear stress-strain conditions obey the following conditions: The yield criterion, the flow and hardening rules, and the crushing condition.

The yield criterion specifies the states of stress at which the plastic flow is initiated. In the case of shells analysis, transverse shear effects are taken into account and therefore a triaxial yield criterion must be employed. DIANA offers the Mohr-Coulomb and Drucker-Prager yield criteria for quasi-brittle materials.

The flow rule specifies the inelastic or plastic strain rate vector as a function of the state of stress. According to the flow theory of plasticity, the plastic strain $\dot{\varepsilon}^p$ is then defined as

Azurém, P – 4800-058 Guimarães Tel. +351 253 510200 • Fax +351 253 510217

$$\dot{\varepsilon}^{p} = \sum_{j=1}^{n} \dot{\lambda}_{j} \frac{\partial g_{j}}{\partial \sigma} \tag{2.13}$$

with λ_j as the plastic multipliers for the n plastic potential functions g_j, which can also be considered as a function of the stress vector σ and an internal state parameter κ, i.e. $g_j(\sigma,\kappa)$. Now the hardening rule specifies the evolution of the internal state parameter, which is generally given as a function of the stress vector and the plastic strain vector, i.e. $\dot{\kappa} = h\left(\sigma, \dot{\varepsilon}^{p}\right)$.

Finally, the crushing condition of the material specifies the type of material fracture, which is given by the ultimate strain of the material.

The plasticity models, whose nonlinear stress-strain conditions have been described above, are formulated by using modern algorithmic plasticity concepts, which include implicit Euler backward and return-mapping schemes.

- Tensile behavior – smeared crack model

Smeared crack models are a combination of tension cut-off, tension softening and shear retention criteria. They can be specified with ambient influence (temperature, concentration or maturity), though they cannot be combined with orthotropic materials.

Smeared crack models basically are formulated with strain decomposition, where the total strain $\dot{\varepsilon}$ is decomposed into an elastic strain $\dot{\varepsilon}^{co}$ and a crack strain $\dot{\varepsilon}^{cr}$ as

$$\dot{\varepsilon} = \dot{\varepsilon}^{co} + \dot{\varepsilon}^{cr} \tag{2.13}$$

As pointed out by de Borst and Nauta (1985), the sub-composition of the crack strain gives the possibility of modeling a number of cracks that simultaneously occur. The basic feature of this multi-directional fixed crack concept, for instance, for a plane strain stress condition, is that a stress $\dot{s}_i$ and strain $\dot{e}_i^{cr}$ exists in the *n-t* coordinate system that is aligned with each crack *i*, see *Figure 2.5*.

Azurém, P – 4800-058 Guimarães Tel. +351 253 510200 • Fax +351 253 510217

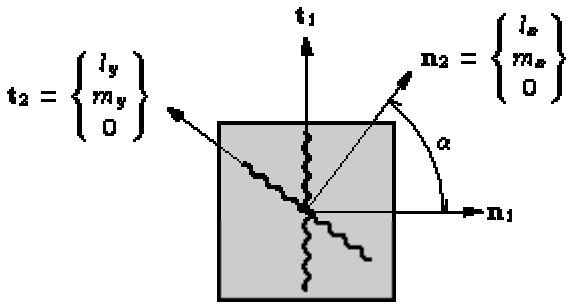

Figure 2.5 - Multi-directional fixed crack model (Plane strain stress condition)

If the vector that assembles the crack strain of each individual crack is denoted by e^{cr}, this yields

$$\dot{e}^{cr} = \left\langle \dot{e}_1^{cr}, \dot{e}_2^{cr}, ..., \dot{e}_i^{cr}, ..., \dot{e}_n^{cr} \right\rangle \tag{2.14}$$

with the crack strain for crack *i* given by $\dot{e}_i^{cr} = \left\langle \dot{\varepsilon}_{nn,i}^{cr}, \dot{\gamma}_{nt}^{cr} \right\rangle$. The relation between the global strain and the vector $\dot{e}^{cr}$ is given by the transformation

$$\dot{\varepsilon}^{cr} = N\dot{e}^{cr} \tag{2.15}$$

being *N* the assembled transformation matrix

$$N = \left[N_1, N_2, ..., N_i, ..., N_n \right] \tag{2.16}$$

and N_i the transformation matrix of crack *i*, which in the case of plane strain is given by

$$N_i = \begin{bmatrix} l_x^2 & l_x l_y \\ m_x^2 & m_x m_y \\ n_x^2 & n_x n_y \\ 2l_x m_x l_y m_y & l_x m_y + l_y m_x \end{bmatrix} \tag{2.17}$$

with $n^T = \{l_x, m_x, n_x\}$ the normalized vector normal to the crack plane. In a similar way it is possible to assemble a vector that contains the stress for each crack as

Azurém, P – 4800-058 Guimarães Tel. +351 253 510200 • Fax +351 253 510217

$$\dot{s}^{cr} = \left\langle \dot{s}_1^{cr}, \dot{s}_1^{cr}, ..., \dot{s}_i^{cr}, ..., \dot{s}_n^{cr} \right\rangle \tag{2.18}$$

with the crack stress for crack *i* given by $\dot{e}_i^{cr} = \left\langle \dot{\sigma}_{nn,i}^{cr}, \dot{\tau}_{nt}^{cr} \right\rangle$. The relation between the global stress and the vector s^{cr} can be derived as

$$\dot{s}^{cr} = N^T \dot{\sigma}^{cr}. \tag{2.19}$$

To complete the system of equations, one needs a constitutive model for the intact concrete and a stress-strain relation for the smeared cracks. For the concrete between the cracks we assume a relationship of the following structure

$$\dot{\sigma} = D^{co} \dot{\varepsilon}^{co}, \tag{2.20}$$

being D^{co} the secant stiffness matrix for the instantaneous moduli of the material. In a similar way, a relation between the crack strain and stress of crack *i* can be defined as

$$\dot{s}_i^{cr} = D_i^{cr} \dot{e}_i^{cr} \tag{2.21}$$

where D_i^{cr} is the secant stiffness matrix for cracking of the material and is defined as

$$D_i^{cr} = \begin{bmatrix} D^I & 0 \\ 0 & D^{II} \end{bmatrix} \tag{2.22}$$

being D^I the mode-I tensile softening modulus and D^{II} the mode-II shear modulus which can be related to the mode-I and mode-II fracture properties of the concrete, respectively.

Finally, it is possible to determine the relation between the stress vector and the strain vector. From the equation of strain decomposition, see Eq. (2.13), the relation for the global stress vector in the global coordinate system can be written as

Azurém, P – 4800-058 Guimarães Tel. +351 253 510200 • Fax +351 253 510217

$$\dot{\sigma} = D\left\{\dot{e} - \dot{e}^{cr}\right\}. \tag{2.23}$$

Introducing Eq. (2.15) into Eq. (2.23) results in

$$\dot{\sigma} = D\left\{\dot{e} - N\dot{\varepsilon}^{cr}\right\}. \tag{2.23}$$

With Eq. (2.21) and after substitution of the relation between the stress vector in the global coordinate system and the stress vector in the crack coordinate system, see Eq. (2.19), the relation is written as

$$\dot{\sigma} = D\left\{\dot{\varepsilon} - N\left[D^{cr}\right]^{-1} N^T \dot{\sigma}\right\} \tag{2.23}$$

which, after some algebraic manipulations, can be written

$$\dot{\sigma} = \left[D - DN\left[D^{cr} + N^T DN\right]^{-1} N^T D\right]\dot{\varepsilon} \tag{2.23}$$

The data format of Elasto-Plastic-Cracking models in DIANA is given according to the following concepts:

- *Tensile behavior*

  Describes the material response in tension, which usually is cracking. DIANA offers the following criteria to describe the tension behavior for Smeared Crack models:

  Tension cut-off

  There are two tension cut-off criteria available in DIANA: constant and linear, see Figure 2.8. Here f_t is the tensile strength and f_c is the compressive strength.

Azurém, P – 4800-058 Guimarães Tel. +351 253 510200 • Fax +351 253 510217

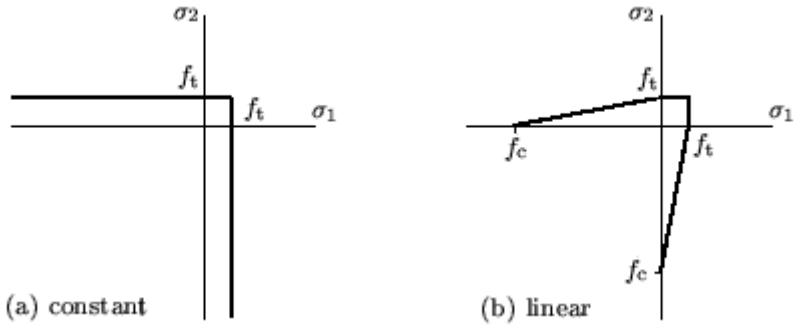

Figure 2.6 - Tension cut-off in two-dimensional principal stress space

Tension softening

Figure 2.7 shows the available tension softening models in DIANA, where ε_u^{cr} is the ultimate strain for cracking, G_f the fracture energy, and h_{cr} is the estimated numerical crack bandwidth.

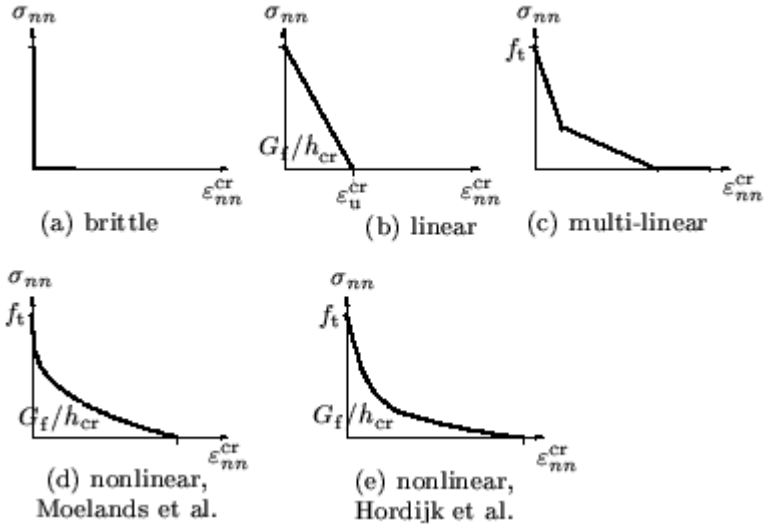

Figure 2.7 - Tension softening - smeared cracks

- *Shear behavior*

Shear retention

Describes how the shear behavior changes when the material is cracked. The modeling of the shear behavior is only necessary in the fixed crack concept where

Azurém, P – 4800-058 Guimarães Tel. +351 253 510200 • Fax +351 253 510217

the shear stiffness G^{cr} is reduced after cracking by a constant shear stiffness reduction β, i.e. $G^{cr} = \beta \cdot G$, being $0 \leq \beta \leq 1$.

- *Compressive behavior*

Describes the crushing behavior of the material. As it has been said, for smeared crack models, the compressive behavior is described by a plasticity model. The data format for the Mohr-Coulomb model and Drucker-Prager models are given below:

YIELD: specifies the criterion to be used: Mohr-Coulomb or Drucker-Prager.

YLDVAL: specifies the yield surface by specifying values for the following parameters: the cohesion c, $sin\phi$ of friction angle ϕ and $sin\psi$ of dilatancy angle ψ.

HARDIA: is the hardening diagram and its definition is specified by the mobilized cohesions c and the corresponding hardening parameters κ.

FRCDIA: specifies a hardening diagram for the friction angle by setting the mobilized friction angles ϕ and the corresponding hardening parameters κ..

DILDIA: specifies plastic dilatancy as a function of the hardening parameter by setting the mobilized dilatancy angle ψ and the corresponding hardening parameters κ.

- *Ambient influence*

Ambient values for temperature, concentration or maturity can be specified. This holds for the YIELD field, where the cohesion c for the Mohr-Coulomb or Drucker-Prager criteria may be specified depending on ambient values.

2.1.2 Crack models based on total strain

Constitutive models based on total strain, also called "Total Strain crack models", describe the tensile and compressive behavior of a material with just one nonlinear relationship (stress-strain relationship). Thus these models do not need a plasticity model to simulate the compressive behavior as smeared crack models do.

In the DIANA program there are two constitutive models based on total strain: the fixed and the rotating strain concepts. These models can neither be combined with other constitutive models, nor with ambient influence. This makes these models well suited for

Azurém, P – 4800-058 Guimarães Tel. +351 253 510200 • Fax +351 253 510217

Serviceability Limit State (SLS) and Ultimate Limit State (ULS) analyses, which are predominantly governed by cracking or crushing of the material.

Within the total strain-stress relationships, various approaches are possible. One commonly used approach is the coaxial stress-strain concept, in which the stress-strain relationships are evaluated in the principal directions of the strain vector. This approach, also known as the *rotating crack model*, is applied to the constitutive modeling of reinforced concrete during a long period and has shown that the modeling approach is well suited for reinforced concrete structures. More appealing to the physical nature of cracking is the *fixed stress-strain concept* in which the stress-strain relationships are evaluated in a fixed coordinate system, which is fixed upon cracking. Both approaches are easily described in the same framework where the crack directions *nst* are either fixed or continuously rotating with the principal directions of the strain vector.

The basic concept of the total strain-based crack models is that the stress is evaluated in the directions, which are given by the crack directions. The strain vector ε_{xyz} in the element coordinate system *xyz* is updated with the strain increment $\Delta\varepsilon_{xyz}$ according to

$$ {}^{+t}\Delta^{t}_{i+1}\varepsilon_{xyz} = {}^{t}\varepsilon_{xyz} + {}^{t+}\Delta^{t}_{i+1}\Delta\varepsilon_{xyz} \tag{2.24} $$

which is transformed to the strain vector in the crack directions with the strain transformation matrix *T*,

$$ {}^{+t}\Delta^{t}_{i+1}\varepsilon_{nst} = T \cdot {}^{t+}\Delta^{t}_{i+1}\Delta\varepsilon_{xyz} \tag{2.25} $$

In a coaxial rotating concept the strain transformation matrix *T* depends on the current strain vector, i.e.,

$$ T = T\left({}^{t+}\Delta^{t}_{i+1}\Delta\varepsilon_{xyz}\right) \tag{2.26} $$

whereas in a fixed concept the strain transformation matrix is fixed upon cracking. The behavior in compression is evaluated in a rotating coordinate system when the material is not cracked, where in case of a fixed concept the compressive behavior is evaluated in the fixed coordinate system determined by the crack directions.

Azurém, P – 4800-058 Guimarães Tel. +351 253 510200 • Fax +351 253 510217

The strain transformation matrix is determined by calculating the eigenvectors of the strain tensor, e.g. with the Jacobi method. The strain tensor is given by

$$E = \begin{bmatrix} \varepsilon_{xx} \\ \varepsilon_{xy} \\ \varepsilon_{xz} \end{bmatrix} \tag{2.27}$$

The eigenvectors are stored in the rotation matrix R that reads

$$R = [nst] = \begin{bmatrix} c_{xx} \\ c_{xy} \\ c_{xz} \end{bmatrix} \tag{2.28}$$

with $c_{xn}=cos\phi_{ij}$ the cosine between the i axis and the j axis. The strain transformation matrix T is then calculated by substituting the appropriate values,

$$T = \begin{bmatrix} c_{xn}^2 & c_{yn}^2 & c_{zn}^2 & c_{xn}c_{yn} & c_{yn}c_{zn} & c_{zn}c_{xn} \\ c_{xs}^2 & c_{ys}^2 & c_{zs}^2 & c_{xs}c_{ys} & c_{ys}c_{zs} & c_{zs}c_{xs} \\ c_{xt}^2 & c_{yt}^2 & c_{zt}^2 & c_{xt}c_{yt} & c_{yt}c_{zt} & c_{zt}c_{xt} \\ 2c_{xn}c_{xs} & 2c_{yn}c_{ys} & 2c_{zn}c_{zs} & c_{xn}c_{ys}+c_{yn}c_{xs} & c_{yn}c_{zs}+c_{zn}c_{ys} & c_{zn}c_{xs}+c_{xn}c_{zs} \\ 2c_{xs}c_{xt} & 2c_{ys}c_{yt} & 2c_{zs}c_{zt} & c_{xs}c_{yt}+c_{ys}c_{xt} & c_{ys}c_{zt}+c_{zs}c_{yt} & c_{zs}c_{xt}+c_{xs}c_{zt} \\ 2c_{xt}c_{xn} & 2c_{yt}c_{yn} & 2c_{zt}c_{zn} & c_{xt}c_{yn}+c_{yt}c_{xn} & c_{yt}c_{zn}+c_{zt}c_{yn} & c_{zt}c_{xn}+c_{xt}c_{zn} \end{bmatrix} \tag{2.28}$$

in a general three-dimensional stress situation. For the other stress situations the appropriate sub-matrix should be taken. The constitutive model is then formulated in the crack coordinate system, which is generally given by

$${}^{+t}\Delta_{i+1}^{t}\sigma_{nst} = \sigma\left({}^{t+}\Delta_{i+1}^{t}\varepsilon_{nst}\right) \tag{2.29}$$

The updated stress vector in the element coordinate system is finally given by

$${}^{+t}\Delta_{i+1}^{t}\sigma_{xyz} = T^{T}\ {}^{t+}\Delta_{i+1}^{t}\sigma_{nst} \tag{2.30}$$

Azurém, P – 4800-058 Guimarães Tel. +351 253 510200 • Fax +351 253 510217

The strain transformation matrix $T^T\left({}^{t+}\Delta^t_{i+1}\varepsilon_{xyz}\right)$ is given by the current strain transformation matrix in the coaxial rotating concept. In a fixed concept the strain transformation matrix T is given by the transformation matrix at the onset of cracking.

The data format of Total Strain crack models in DIANA is given according to the following concepts:

- Type of Total Strain model to be used: Fixed or Rotate
- Basic properties (tensile, shear and compressive behaviors and lateral influence): they can be derived from Model Code regulations, e.g. CEB-FIB model, or they can be defined by direct input as follows:

Tensile behavior

Describes the material response in tension, which usually is cracking. DIANA offers a set of predefined softening functions as shown in Figure 2.8 to describe the tensile behavior. Here, the parameter G_f^I is the Mode-I fracture energy.

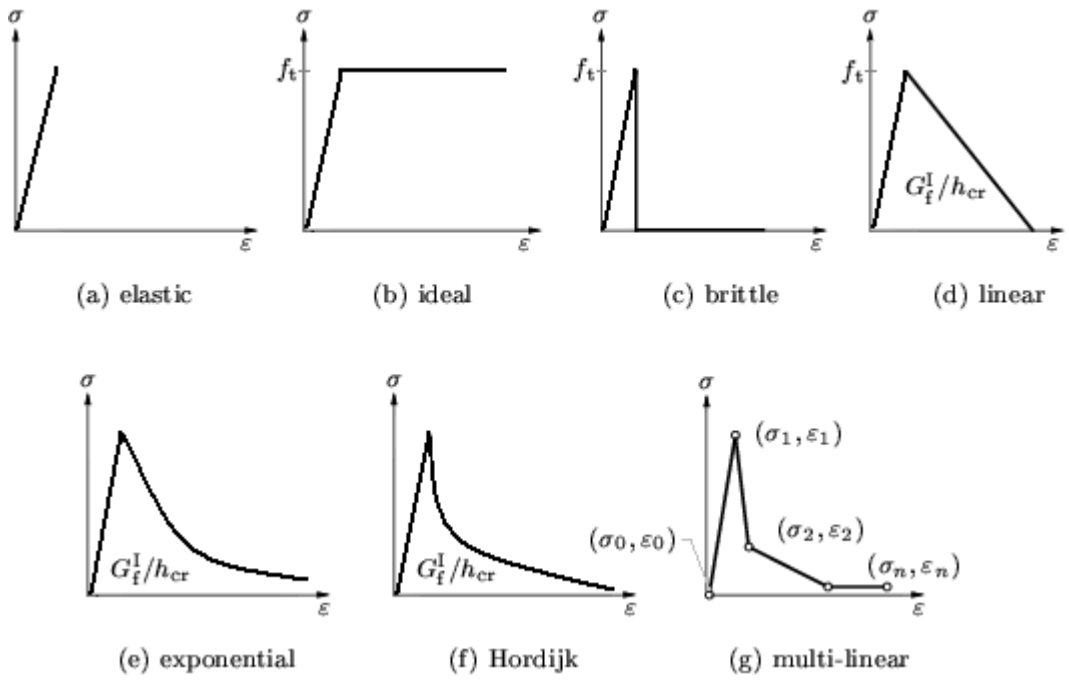

Figure 2.8 - Pre-defined tension softening for total strain model.

Azurém, P – 4800-058 Guimarães Tel. +351 253 510200 • Fax +351 253 510217

Shear behavior

See the Elasto-Plastic-Cracking models.

Compressive behavior

Describes the crushing behavior of the material within the same concept as the tensile behavior. Therefore the compression parameters are specified depending on the compression function as outlined in Figure 2.9. Here, f_{co} is the initial compressive strength, $f_{c\infty}$ is the ultimate compressive strength at infinite strain, G_c is the compressive fracture energy, γ is the decaying factor, and E_{har} is the constant hardening modulus.

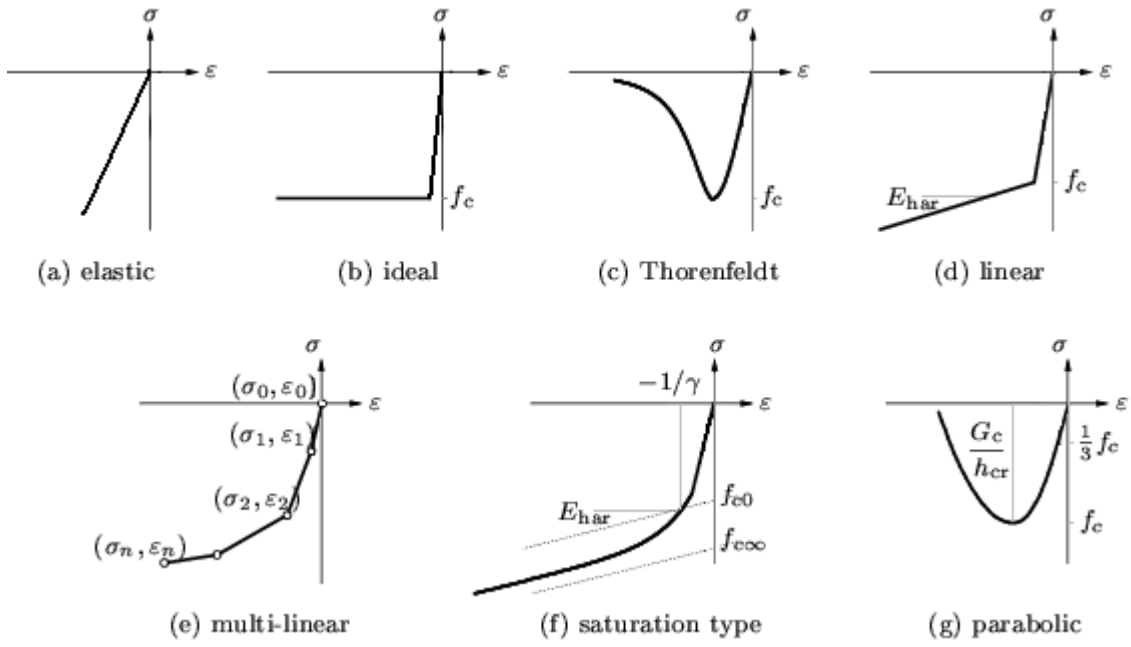

Figure 2.9 - Pre-defined compression behavior for total strain model

Lateral influence

Models may be applied within a concept based on total strain to describe the effect of lateral cracking or lateral confinement.

Azurém, P – 4800-058 Guimarães Tel. +351 253 510200 • Fax +351 253 510217

3 Analysis of Reinforced Masonry Shells

The reinforced masonry shells analyzed here have been tested by Sarrablo (2002). Each masonry shell, supported on a metallic support that simulates pinned supports, was tested experimentally by applying a single concentrated load *P*, at a quarter span, see *Figure 3.1a,b*. Two layers constitute the masonry shell, being the first layer mortar (upper) and the second layer masonry (lower), (see *Figure 3.1c*). The masonry layer is made of hollow clay blocks and reinforcement bars, in the transverse and longitudinal joints (see *Figure 3.1d*). The geometry of the shells follows a catenary shape, with a directrix shown in *Figure 3.1e*.

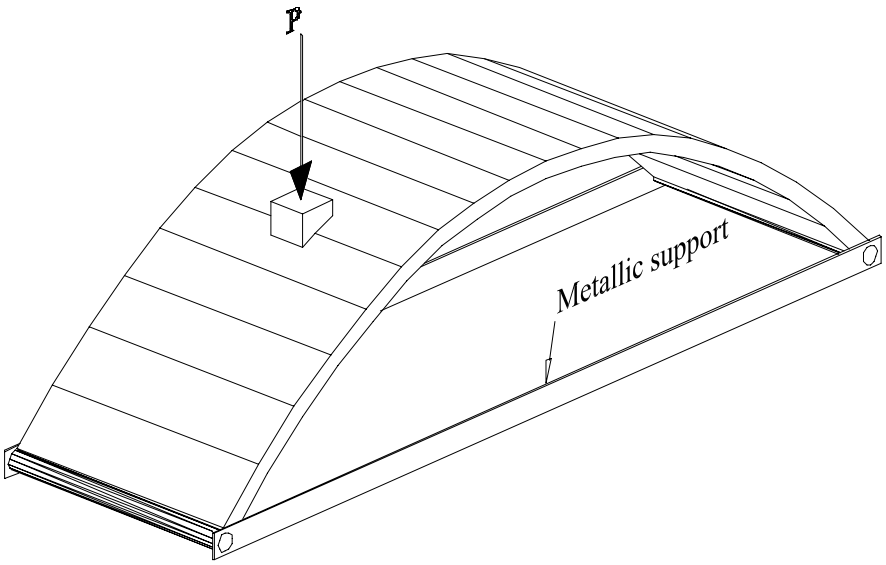

(a)

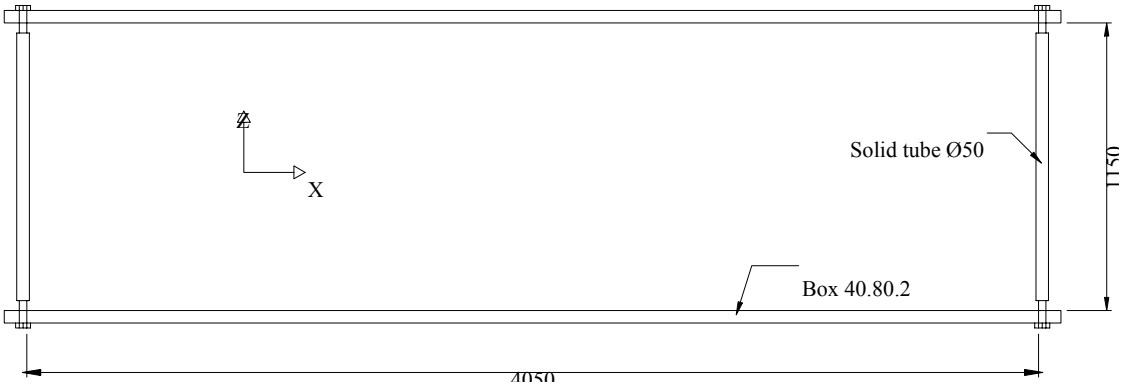

(b)

Azurém, P – 4800-058 Guimarães Tel. +351 253 510200 • Fax +351 253 510217

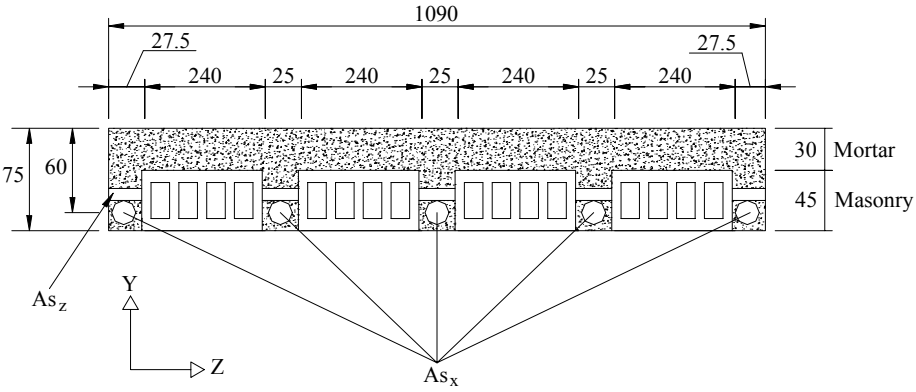

(c)

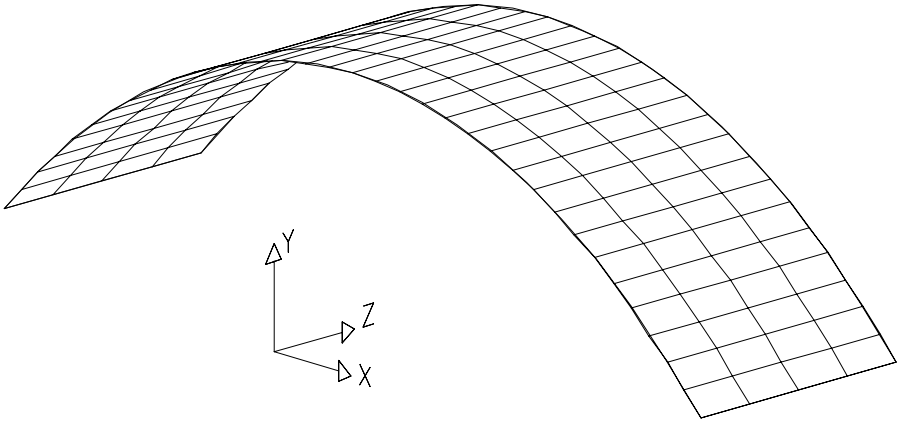

(d)

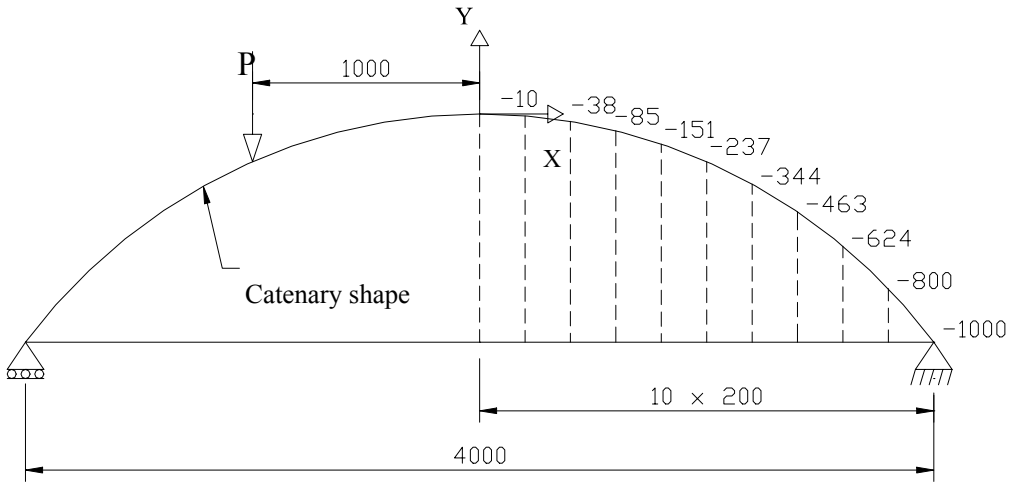

(e)

Figure 3.1– Shell series in consideration with point load *P* (units in millimeter), Sarrablo (2002) : (a) experimental set-up; (b) plan view of the metallic support; (c) cross section; (d) lower reinforcement mesh; (e) geometry of the catenary

Azurém, P – 4800-058 Guimarães Tel. +351 253 510200 • Fax +351 253 510217

Both layers of the shells were modeled using the Total Strain crack model (fixed concept) referred before. This model was selected due to wide availability, robustness and the fact that the load is applied monotonically. The reinforcement mesh was modeled with the embedded reinforcement types available in DIANA, with a Von Mises yield criterion.

With reference to the input data for the material models, *Table 3.1* and *Table 3.2* present the adopted elastic and inelastic material properties that were used for masonry and mortar layers, respectively. These values have been obtained from Sarralbo (2002) and other considerations, see Annex A.

Table 3.1 – Material properties for masonry layer

Elastic properties		
Shell	E N/mm^2	ν -
All	14000	0.2

Inelastic properties					
Shell	Mortar	f_m N/mm^2	G_{fc} N/mm	f_t N/mm^2	G_f N/m
1 / 2	1	13.6	20	0.74	5.3
3	3	19.6	22	0.90	9.8
4	4	19.3	22	0.88	9.5
5	5	16.5	21	0.83	7.1

Table 3.2 – Material properties for mortar layer

Shell	Mortar	Mortar Strength*	f_{cm} N/mm^2	E N/mm^2	ν -	f_{tm} N/mm^2	G_{fm} N/m	G_{fcm} N/mm
1 / 2	2	Low	16.8	25600	0.2	1.29	36	21
3	3	High	45.0	35500	0.2	2.20**	72	27
4	4	High	42.8	34900	0.2	2.00	69	27
5	6	Low	30.9	31300	0.2	1.70	55	25

* Classification given by Sarrablo (2002)
** Estimated

Azurém, P – 4800-058 Guimarães Tel. +351 253 510200 • Fax +351 253 510217

For the reinforcement mesh, *Table 3.3* presents the geometry and material properties. Here As_x and As_z are steel areas in the x and z directions, respectively, f_y is the yield strength of the reinforcement (assumed from the Steel Class, as no tests have been carried out), E is the Young's modulus and, ν is the Poisson's ratio.

Table 3.3 – Reinforcement data for the shell series

Shell	Reinforcement							
	Longitudinal			Transversal			Mechanical properties	
	N°. of bars	As_x (mm^2)	f_y (N/mm^2)	N°. of bars	As_z (mm^2)	f_y (N/mm^2)	E (N/mm^2)	ν
1 / 2	5 ϕ 8	251.3	500	37 ϕ 6	1046.2	400	200000	0.2
3	5 ϕ 8	251.3	500	37 ϕ 6	1046.2	400	200000	0.2
4	5 ϕ 6	141.4	400	37 ϕ 6	1046.2	400	200000	0.2
5	5 ϕ 6	141.4	400	37 ϕ 6	1046.2	400	200000	0.2

With reference to the experimental results obtained by Sarrablo (2002) for the shell series, *Table 3.4* shows the material strengths and the collapse loads for the shell series, and *Figure 3.2* shows the load-displacement diagrams for a vertical displacement d at the point of application of load P.

Table 3.4 – Mortar strength and ultimate loads for shell series tested by Sarrablo

Shell	Mortar strength for compression (MPa)		Ultimate load (kN)
	Upper layer	Joints	
2	16.8	10.4	21.0
3	45.0	45.0	26.0
4	42.8	42.8	15.2
5	30.9	22.6	14.2

Azurém, P – 4800-058 Guimarães Tel. +351 253 510200 • Fax +351 253 510217

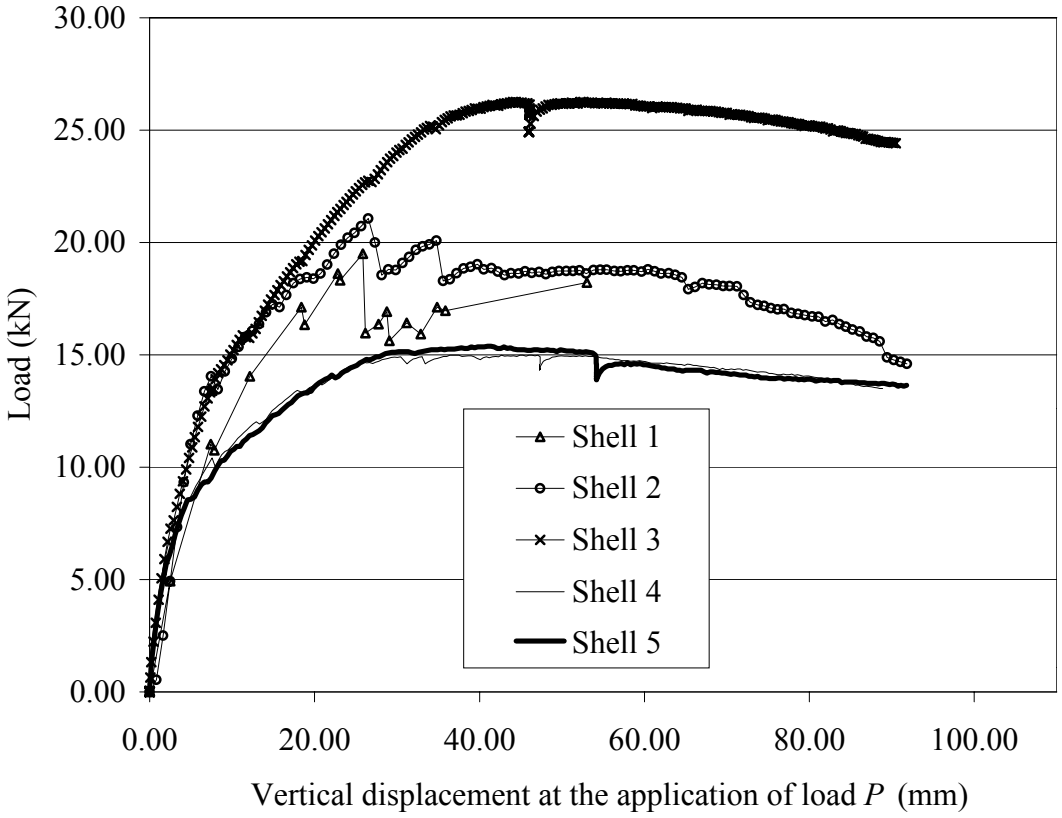

Figure 3.2 – Load-displacement diagrams for shell series tested by Sarrablo (2002)

3.1 Numerical Results with a Plane Stress Model

Given the one-dimensional character of the structure, eight-node quadrilateral isoparametric plane stress elements with two in-plane Gauss integration have been adopted for the analysis, together with embedded mesh elements for the reinforcement. The analyses were performed with arc-length control enhanced with lines searches, aiming at a globally convergent algorithm.

Figure 3.3 shows the numerical results for shell series 1 / 2, at ultimate stage, in terms of vertical displacements, bending moments, membrane forces and load-displacement diagrams, at the point of application of the load *P*. The load-displacement diagrams include the numerical results, the experimental results and the limit load value of Palacio et al. (2003).

Azurém, P – 4800-058 Guimarães Tel. +351 253 510200 • Fax +351 253 510217

The experimental results are in very good agreement with the numerical results, in terms of collapse load and arch behavior. *Figure 3.3*a shows the typical four-hinged collapse mechanism found in the experiments and adopted for limit analysis. The very ductile response of the shell is due to the yielding of reinforcement at the left hinge, previous to mortar crushing. As shown in *Figure 3.3*e, the initial stiffness obtained in the numerical analysis is rather high, followed by a sharp drop of strength, associated with cracking of the right hinge. This is confirmed by Sarralbo (2002), who refers cracking of the right hinge as the first sign of inelastic behavior. It is noted that the first peak and high stiffness do not occur in the experimental tests, which is probably due to a very low tensile strength of the upper layer, related to the difficulties in placing the mortar.

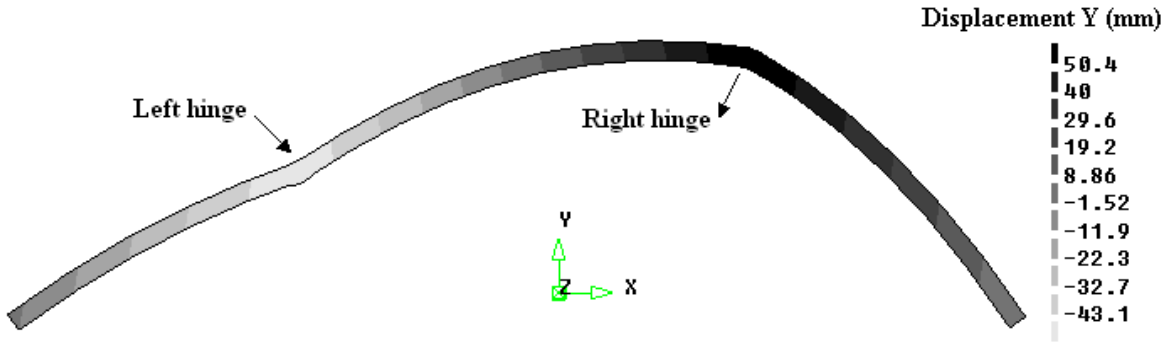

(a)

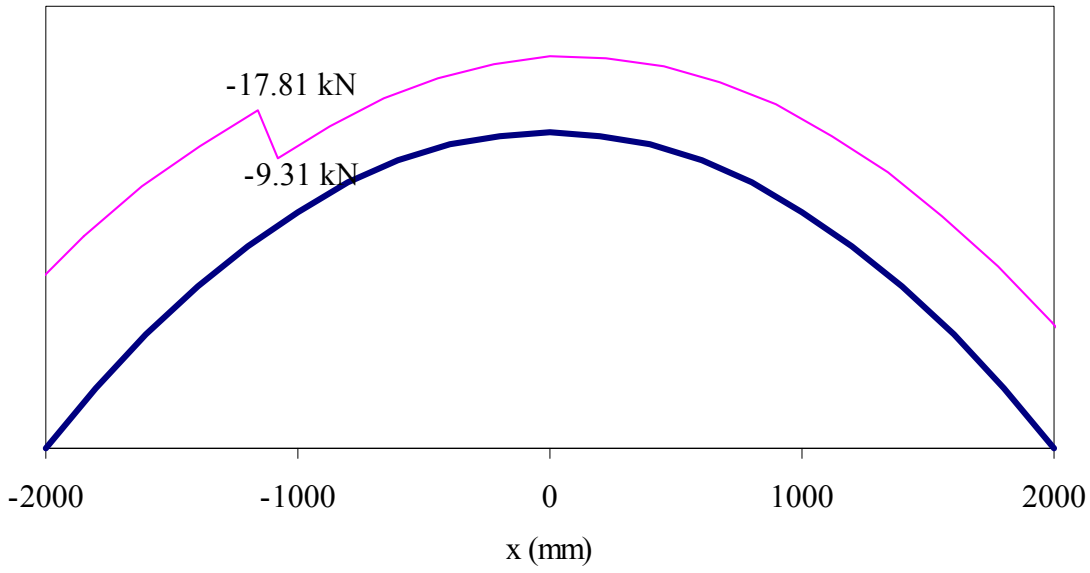

(b)

Azurém, P – 4800-058 Guimarães Tel. +351 253 510200 • Fax +351 253 510217

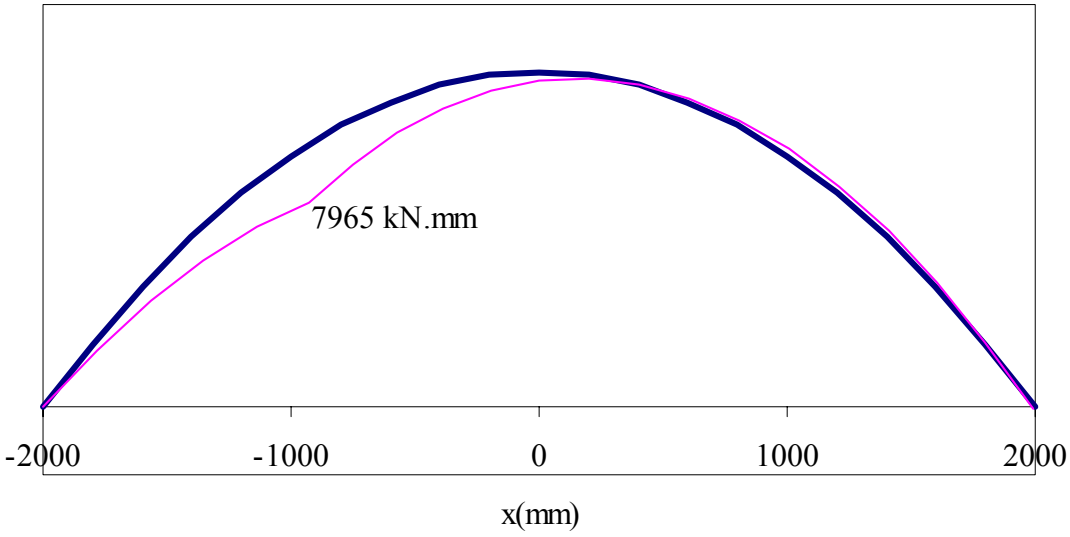

(d)

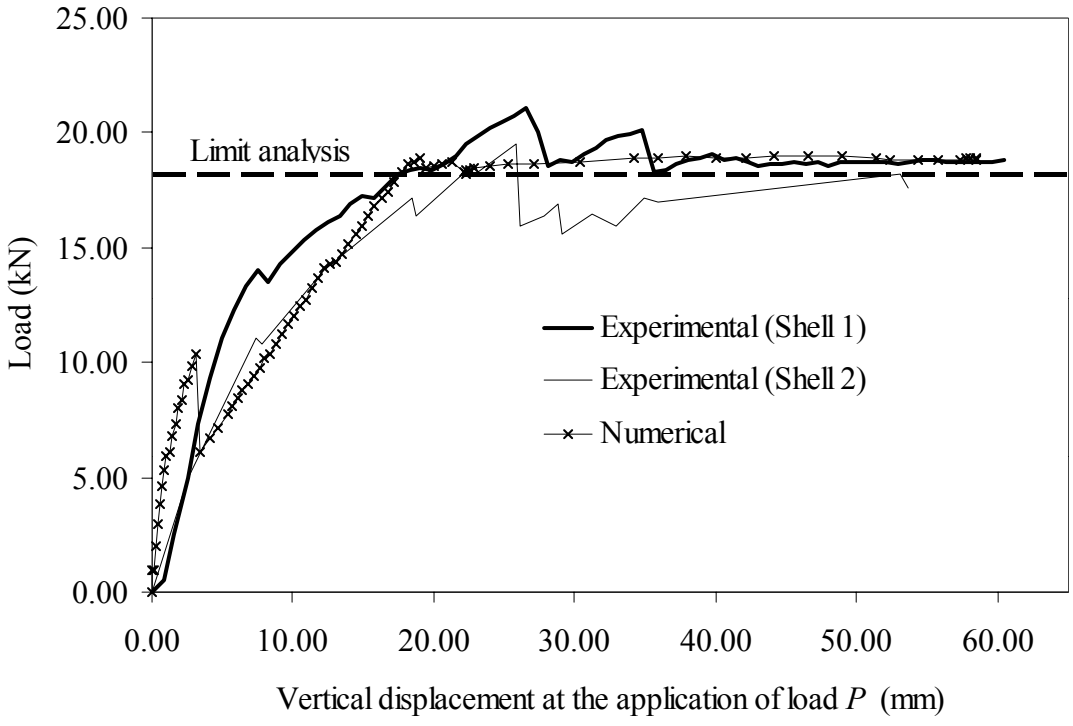

(e)

Figure 3.3 – Shell series 1 / 2. Results of the analysis at a load *P* equal to 19.0 kN (peak): (a) total deformed shape; (b) bending moment diagram; (c) normal force diagram; (d) experimental and numerical load-displacement diagrams.

Azurém, P – 4800-058 Guimarães Tel. +351 253 510200 • Fax +351 253 510217

Finally, it is also noted that the post-cracked stiffness of the numerical results deviates from the experimental values, which is attributed to the bond-slip behavior of the reinforcement, set in a very narrow mortar joint.

Figure 3.4 shows the results for shell series 3, again, in terms of vertical displacements, bending moments, membrane forces and load-displacement diagrams, at the point of application of the load *P*. The behavior of this shell is similar to the previous shell. But, in this case, there is approximately 20% difference between the calculated and observed failure load. It is striking that the value obtained with the limit analysis is rather close to the value obtained with the sophisticated non-linear analysis. Due to this agreement, it is possible to conclude that the yield strength of steel is responsible for the differences found in the results. The characterization of the yield strength of steel is therefore needed for all tests in course.

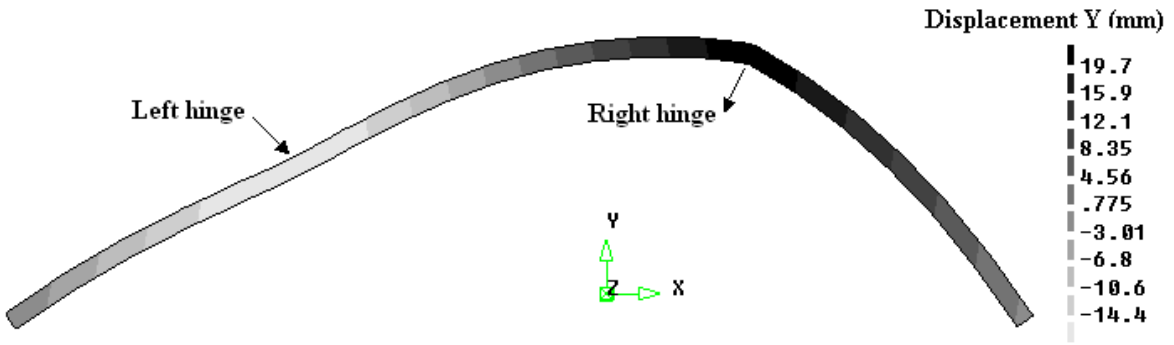

(a)

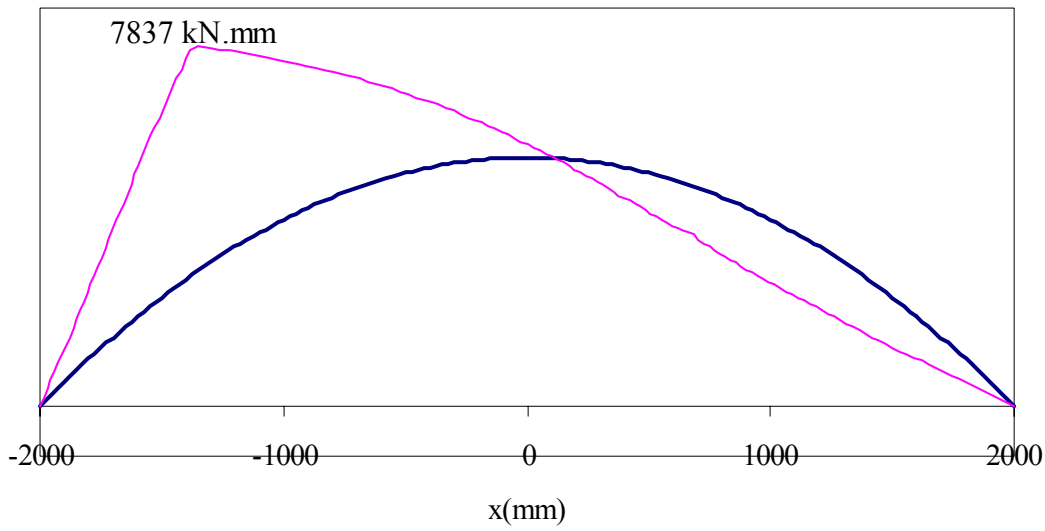

(b)

Azurém, P – 4800-058 Guimarães Tel. +351 253 510200 • Fax +351 253 510217

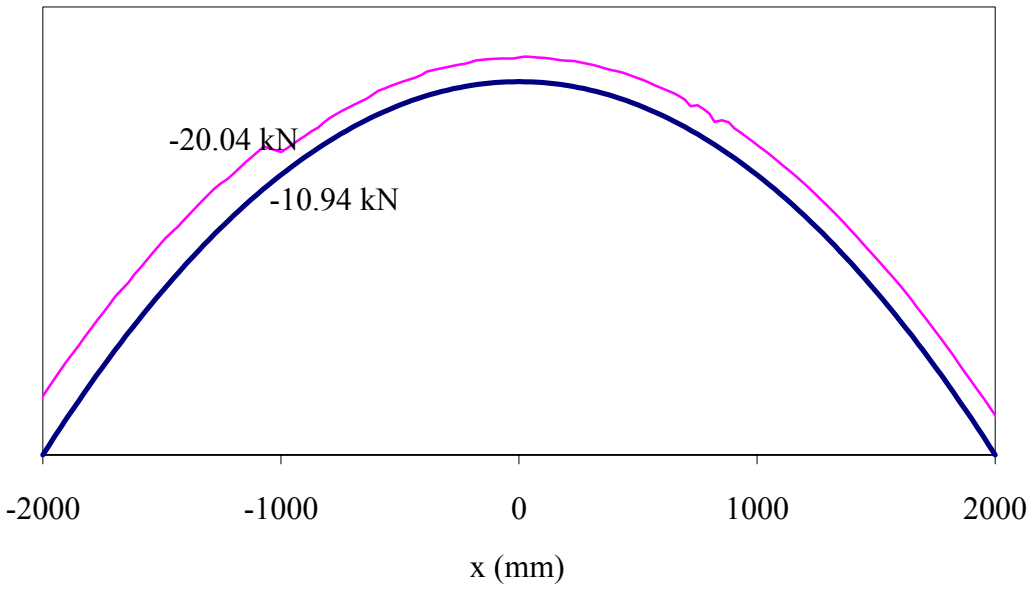

(c)

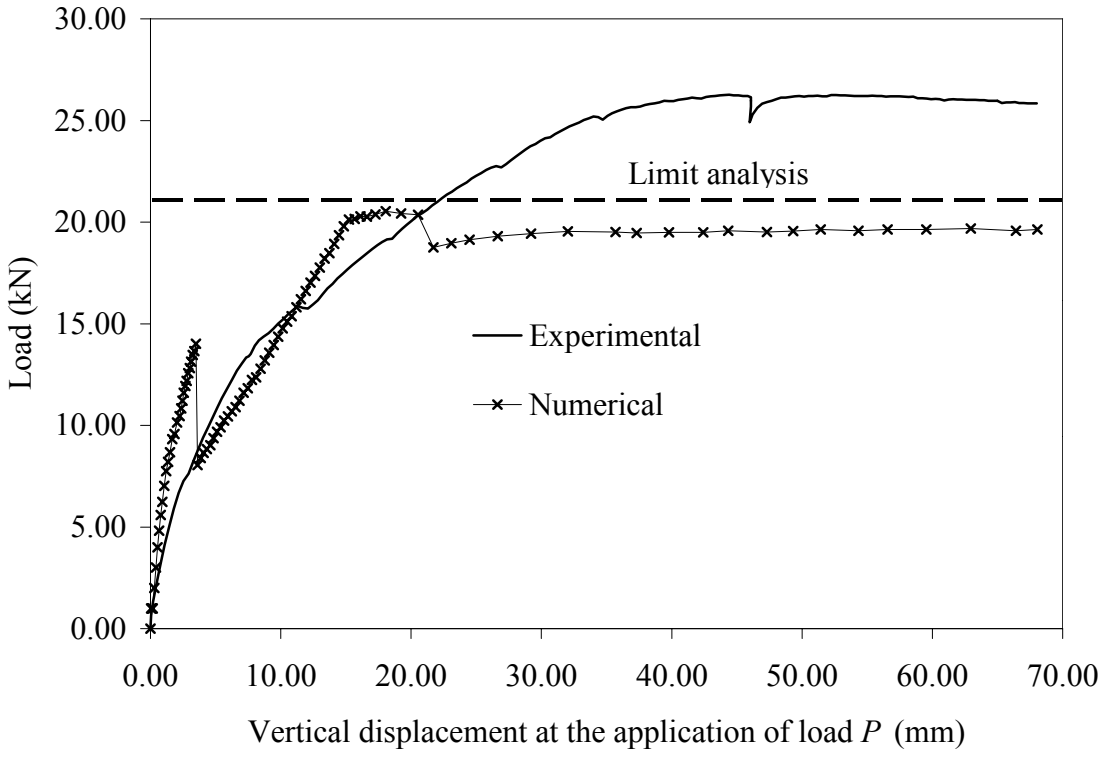

(d)

Figure 3.4– Shell series 3. Results of the analysis at a load *P* equal to 20.5 kN (peak): (a) total deformed shape; (b) bending moment diagram; (c) normal force diagram; (d) Experimental and numerical load-displacement diagrams.

Azurém, P – 4800-058 Guimarães
Tel. +351 253 510200 • Fax +351 253 510217

Figure 3.5 shows the results for shell series 4, again, in terms of vertical displacements, bending moments, membrane forces and load-displacement diagrams, at the point of application of the load *P*. The behavior of this shell is similar to the previous shell but the cracking load is higher than the residual plateau load. This can be clearly observed in *Figure 3.5*a, where it can be seen that the right hinge has note yet cracked. After cracking of the right hinge and yielding of the reinforcement, the typical four-hinged collapse mechanism is found, see *Figure 3.6*.

Again, significant difference is found between the calculated and observed failure load, due to the lack of information on the constitutive behavior of steel. It is noted that the value obtained with the limit analysis is rather close to the cracking value but unsafe, with respect to the ductile-yield value. It is therefore recommended that the procedure propose in Palácio et al. (2003) is not adopted for design, if the cracking load is higher than the load associated with yielding of the reinforcement.

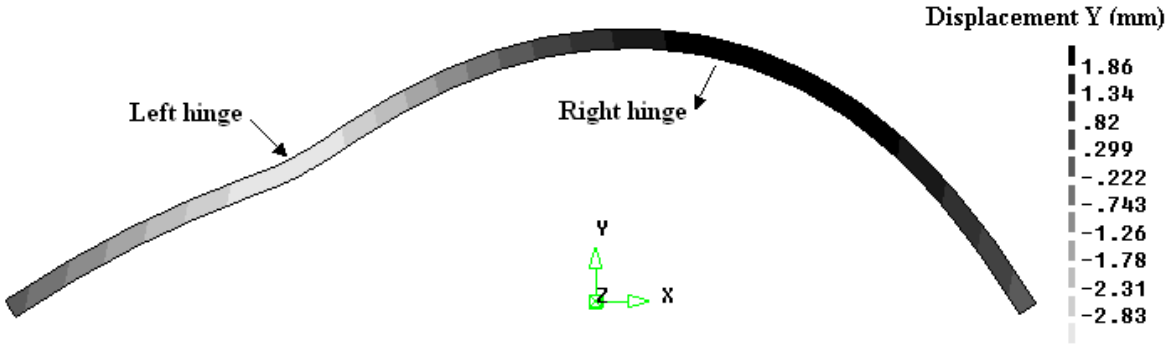

(a)

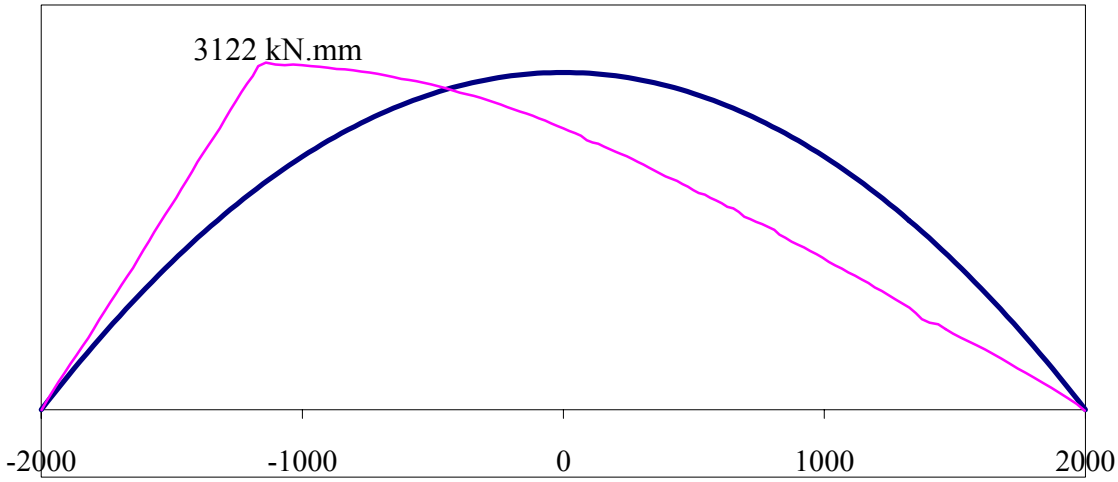

(b)

Azurém, P – 4800-058 Guimarães Tel. +351 253 510200 • Fax +351 253 510217

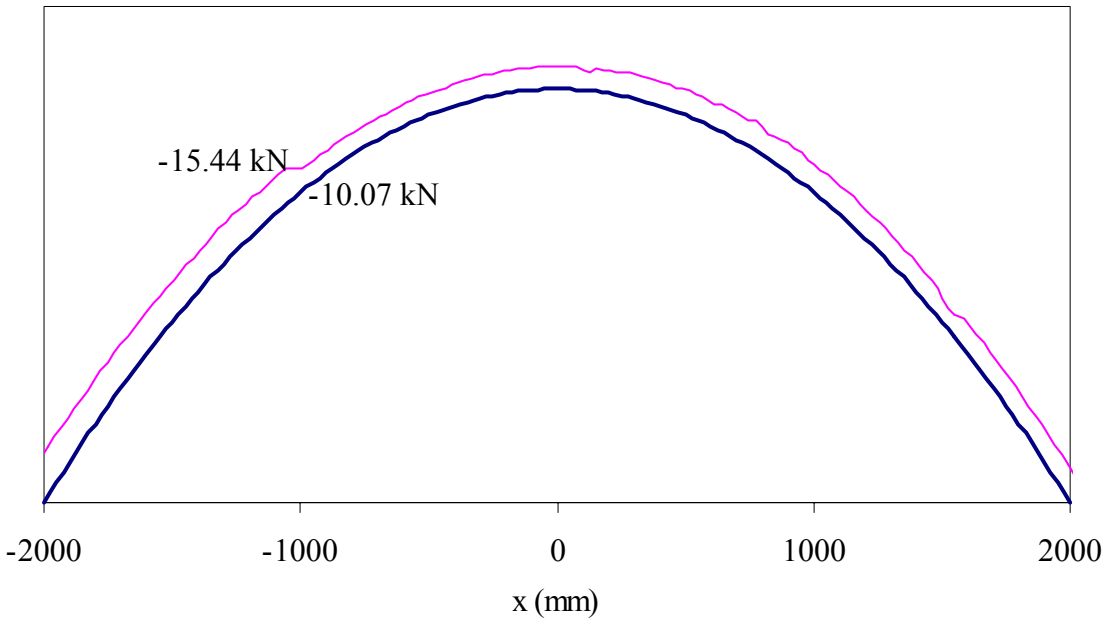

(c)

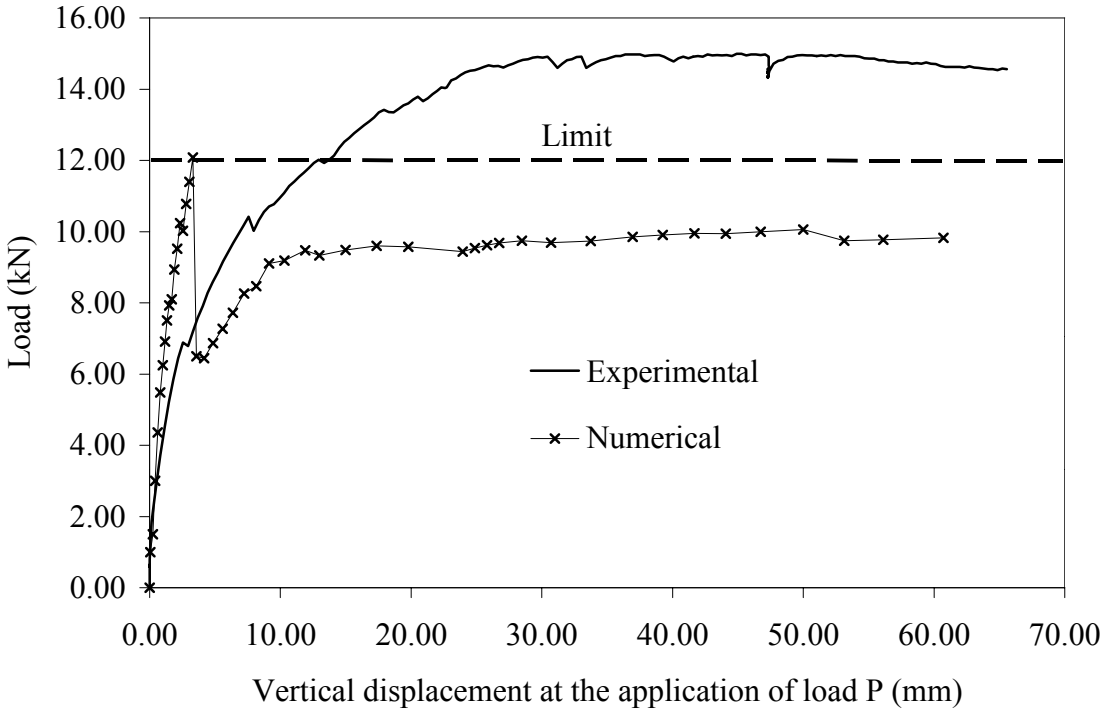

(d)

Figure 3.5– Shell series 4. Results of the analysis at a load *P* equal to 12.1 kN (peak): (a) total deformed shape; (b) bending moment diagram; (c) normal force diagram; (d) experimental and numerical load-displacement diagrams.

Azurém, P – 4800-058 Guimarães
Tel. +351 253 510200 • Fax +351 253 510217

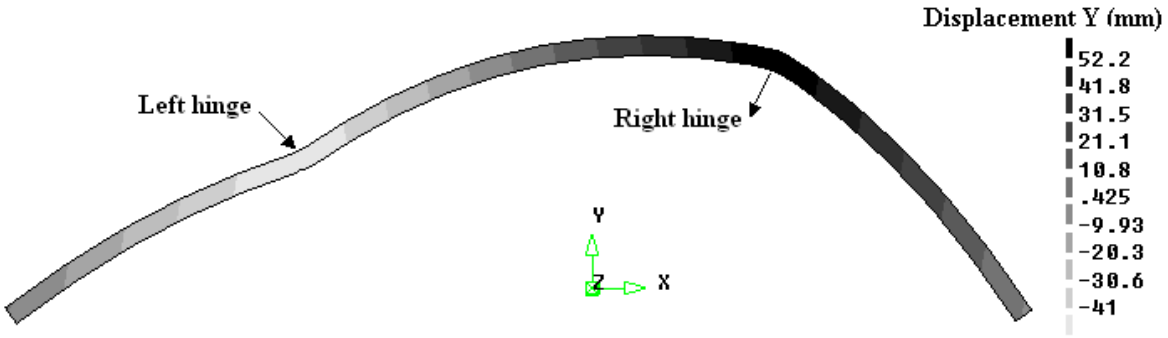

Figure 3.6 - Shell series 4. Deformed shape for load *P* equal to 10.1 kN (pos-peak load).

Finally, *Figure 3.7* shows the results for shell series 5, again, in terms of vertical displacements, bending moments, membrane forces and load-displacement diagrams, at the point of application of the load *P*. The behavior of this shell is similar to the other shells, again with reasonable agreement between limit analysis and the numerical results. The experimental results deviate again from both analyses.

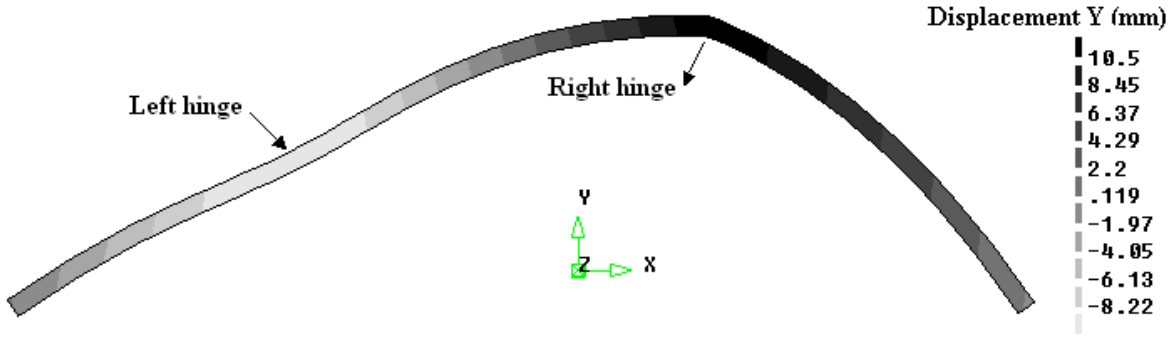

(a)

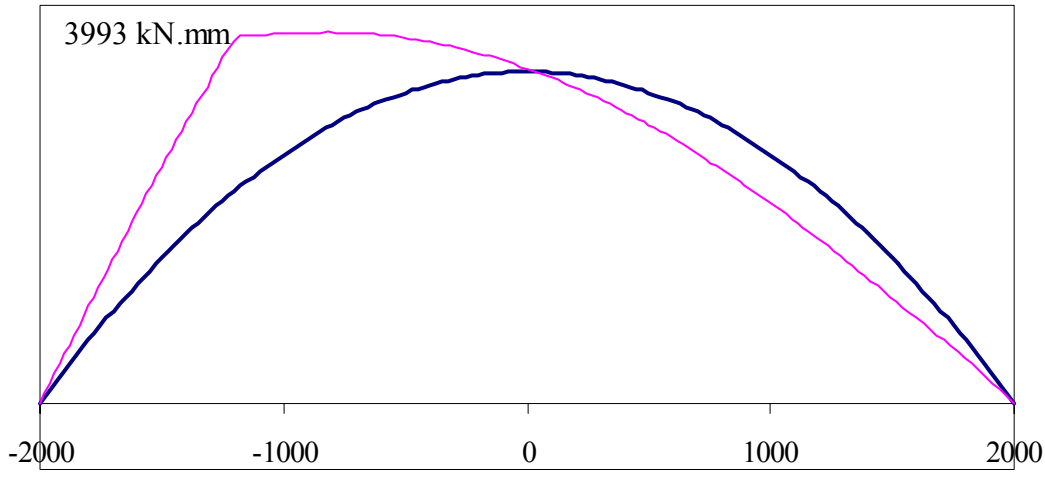

(b)

Azurém, P – 4800-058 Guimarães
Tel. +351 253 510200 • Fax +351 253 510217

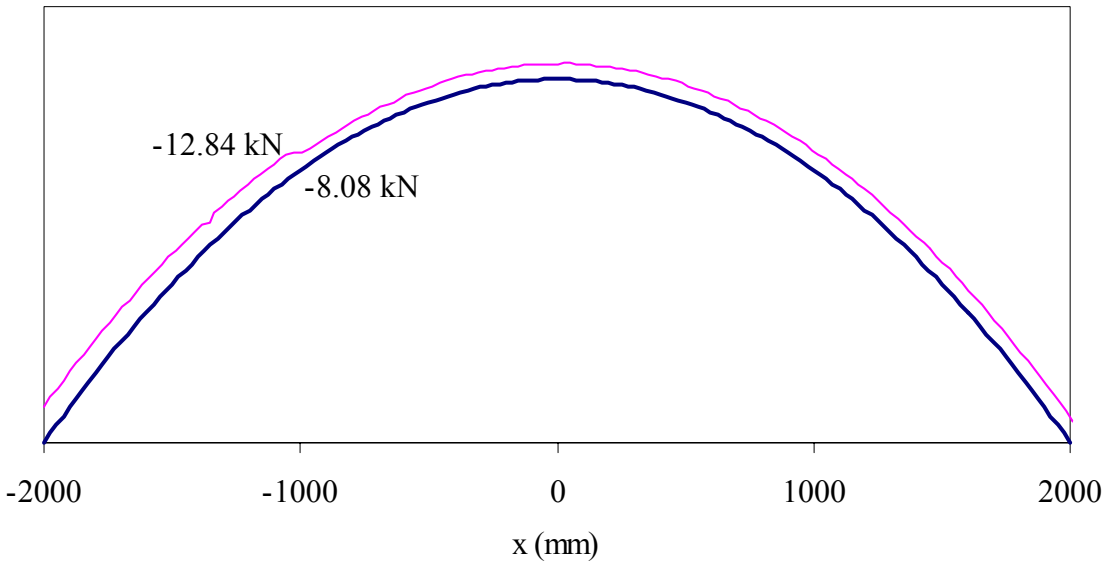

(c)

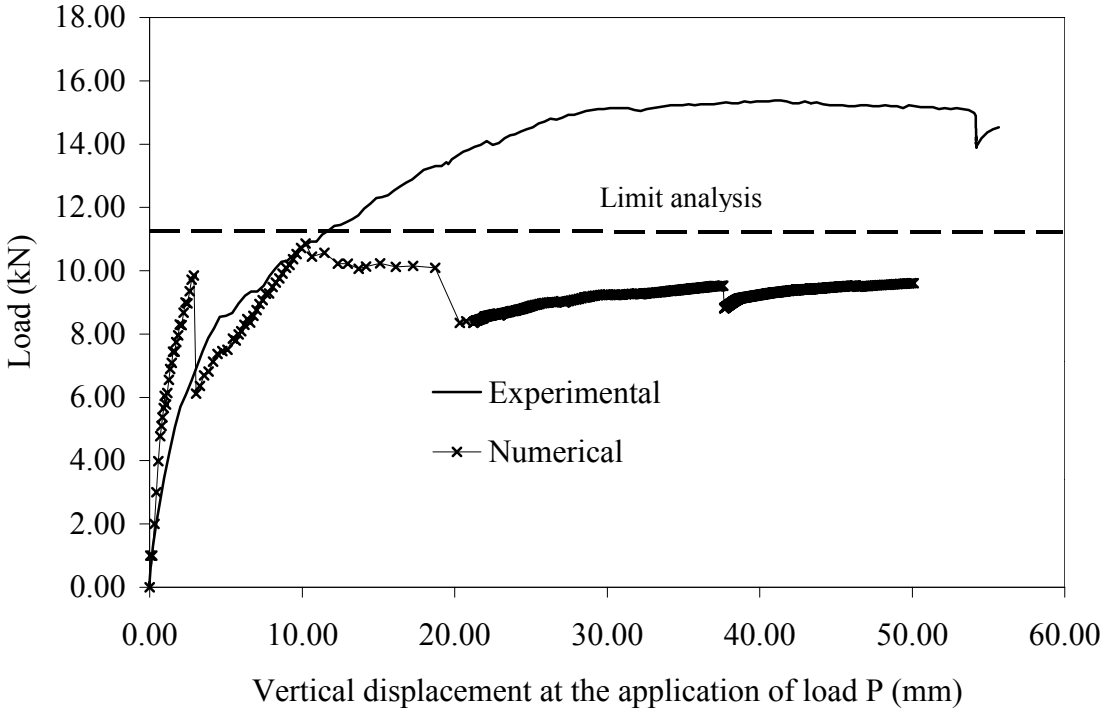

(d)

Figure 3.7 – Shell series 5. Results of the analysis at a load *P* equal to 10.86 kN (peak): (a) total deformed shape; (b) bending moment diagram; (c) Normal force diagram; (d) experimental and numerical load-displacement diagrams.

Azurém, P – 4800-058 Guimarães Tel. +351 253 510200 • Fax +351 253 510217

3.3 Sensitivity Analysis

As it was discussed in Palacio *et al* (2003), the lack of experimental information on the reinforcement steel and possible lack of reliability on the tensile properties of mortar, which were determined by Sarrablo (2002), are the likely reasons for the disagreements found in the previous section. In order to evaluate the influence of mechanical properties of mortar and masonry on the structural behavior of the shells analyzed before, two additional analyses have been carried out for shell series 3.

In the first analysis the tensile behavior was assumed ideally plastic whereas, in the second analysis, the compressive behavior was assumed ideally plastic. The new load-displacement diagrams are shown in *Figure 3.8*. As it can be observed in this figure, the change in the tensile properties values dramatically affects the response but the change in the compressive properties values does not affect the response. The results confirm the hypotheses rose in Palacio et al (2003), with relation to the influence of the tensile strength and yield strength of reinforcement on the structural behavior of the shells.

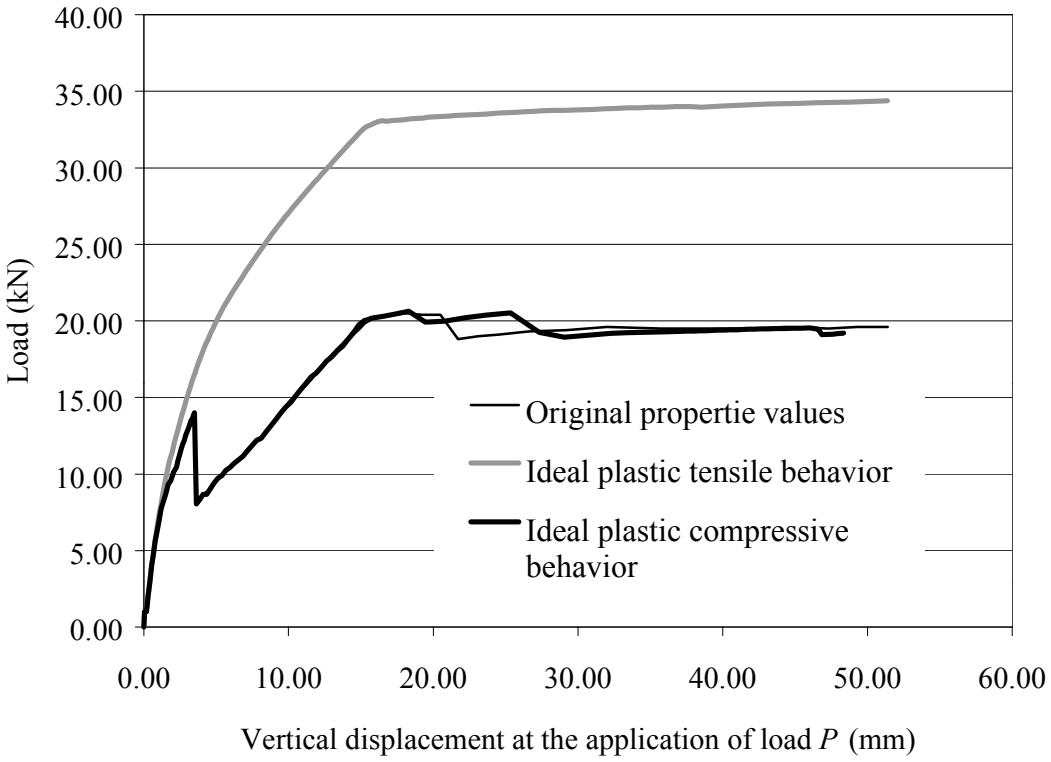

Figure 3.8– Load-displacements diagrams for the verification of the influence of mechanical properties of shell series 3.

Azurém, P – 4800-058 Guimarães Tel. +351 253 510200 • Fax +351 253 510217

4 Conclusions

The numerical analysis performed with non-linear finite elements, with respect to the structural behavior of the shell series tested by Sarrablo (2002), did not show good agreement with the experimental results. Due to the large influence of the tensile strength of the shells and of the yield strength of the reinforcement in the results, it is recommended that additional effort be made in such direction.

The post-peak behavior of the shells seems not to be well reproduced by the model. It is recommended that the bond-slip behavior of the reinforcement in studied in more detail, as this is the probable cause for the anomaly detected.

The procedure established in Palácio et al. (2003) for the limit analysis of reinforced masonry shells seems adequate but provisions are required to ensure that a ductile post-peak behavior is obtained.

Azurém, P – 4800-058 Guimarães Tel. +351 253 510200 • Fax +351 253 510217

5 References

BERTO, L., SAETTA, A., SCOTTA, R., VITALIANI, R. (2002) - Orthotropic damage model for masonry structures. International Journal for Numerical Methods in Engineering, 55(2), 127–157.

CEB (1993) - CEB-FIP Model Code 1990, Bulletin d'Information nº 213/214, Thomas Telford, London, UK.

de BORST, R., NAUTA, P. (1985) – Non-orthogonal cracks in a smeared finite element model, Eng. Comput. 2., 35–46.

DHANASEKAR, M., PAGE, A.W., KLEEMAN, P.W. (1985) - The failure of brick masonry under biaxial stresses. Proc. Intsn. Civ. Engrs., Part 2., 79, 295–313.

LOURENÇO, P.B. (1996) – A user / programmer guide for the micro-modelling of masonry structures, Report TU-DELFT nº 03.21.1.31.35, Delft University of Technology, Delft, The Netherlands.

LOURENÇO, P.B., ROTS, J.G., BLAAUWENDRAAD, J. (1998) - Continuum model for masonry: Parameter estimation and validation. Journal of Structural Engineering, ASCE, 124(6), 642-652.

LOURENÇO, P.B., BARROS, J.O., ALMEIDA, J.C. (2002) - Characterization of masonry under uniaxial tension, Report nº 02-DEC/E-12, Universidade do Minho, Guimarães, Portugal.

OLIVEIRA, J.T., LOURENÇO, P.B., BARROS, J.O. (2002) - Shear testing of stacked bonded masonry, Report nº 02-DEC/E-10, Universidade do Minho, Guimarães, Portugal.

PALACIO, K., LOURENÇO, P.B., BARROS, J.O. (2003) - Contribution to Design Criteria for Industrialized Masonry Vaults, Report nº 03-DEC/E-10, Universidade do Minho, Guimarães, Portugal.

van der PLUIJM, R. (1999) - Out of plane bending of masonry behavior and strength, PhD Thesis, Eindhoven University of Technology, Eindhoven, the Netherlands.

RASHID, Y. R. (1968) – Analysis of prestressed concrete pressure vessels, Nuclear Eng. Des. 7, 334-344.

Azurém, P – 4800-058 Guimarães Tel. +351 253 510200 • Fax +351 253 510217

SARRALBO, V. (2002) - Contribution to the viability of laminar reinforced masonry roofs using semi-prefabricated solutions. Proposal for short span cylindrical shells (in Spanish), PhD Thesis, Universitat Politècnica de Catalunya, Barcelona, Spain.

TNO Building and Construction Research (2003) – User's manual of material library, Release 8.1, Department of Computational Mechanics, Delft, The Netherlands.

VECCHIO, F. J., COLLINS, M. P(1986) - The modified compression field theory for reinforced concrete elements subjected to shear, ACI Journal 83, 22, 219-231.

Azurém, P – 4800-058 Guimarães Tel. +351 253 510200 • Fax +351 253 510217

ANNEX A

Justification of the Adopted Material Properties

The geometry of the reinforced masonry shells is illustrated in Figure A.1, both in plan view and cross section. For the purpose of numerical analysis it is necessary to define the material axes of orthotropy. Here, it is defined that the *x* axis is oriented along the shell span, the z axis is transverse to the shell span and the y axis is oriented along the thickness of the shell. As it has been said, two layers are considered through the thickness of the shell, Layer 1, which is solely made of mortar, and Layer 2, which is made of stack bonded masonry.

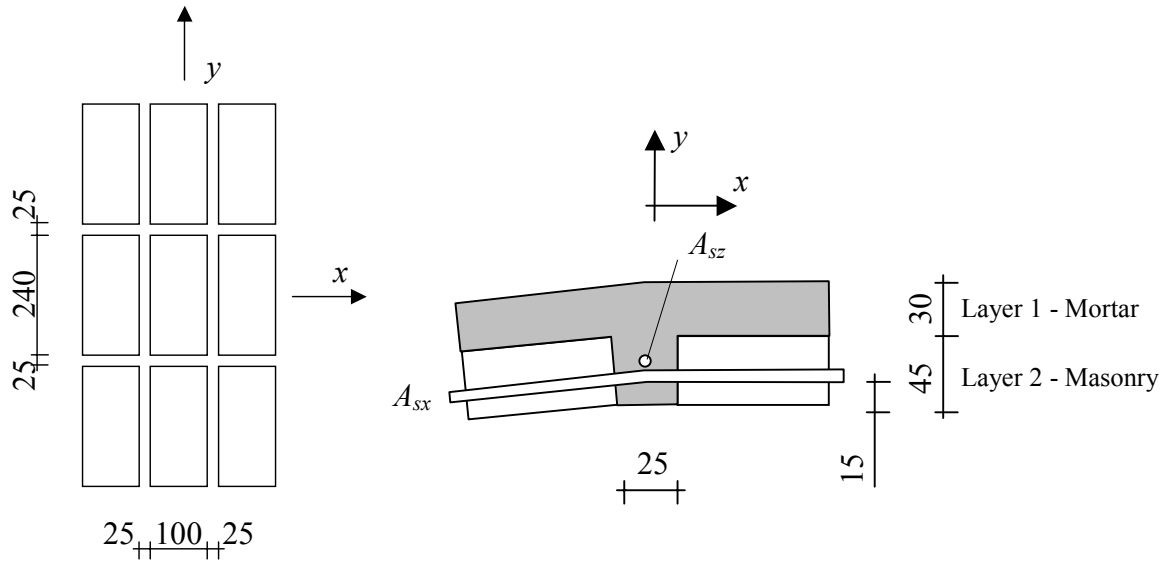

Figure A.1 – Definitions and geometry: (a) material axes – plan view; (b) layers – cross section

Azurém, P – 4800-058 Guimarães Tel. +351 253 510200 • Fax +351 253 510217

A.1 Mechanical properties for mortar

Mortar can be assumed to behave as an isotopic material, similar to concrete. From the average compressive strength of the mortar f_m, the material data for the mortar required for advanced non-linear calculations, will be estimated from the following hypothesis, see CEB-FIP (1993):

- The real compressive strength of mortar f_{cm} is equal to 0.8 f_m, because the values indicated from Sarralbo (2002) were carried out in mortar cubes prepared according to EN 1015-11;
- The Young modulus E_m is equal to $21500 \times (f_{cm} / 10)^{1/3}$;
- The Poisson coefficient ν_m is equal to 0.2;
- The tensile strength f_{tm} is equal to $1.4 \times [\ (f_{cm} - 8) / 10\ ]^{2/3}$, tests have not been carried out (series 1 and 2);
- The fracture energy of the mortar G_{fm} is assumed equivalent to the value for concrete of maximum aggregate size 8 mm, being equal to $0.025 \times (f_{cm} / 10)^{0.7}$;
- The fracture energy of the mortar in compression G_{fcm} is assumed equivalent to the value for concrete, resulting from the integration of the stress-strain curves in the expression $15 + 0.43\, f_{cm} - 0.0036\, (f_{cm})^2$, see *Figure A.2*.

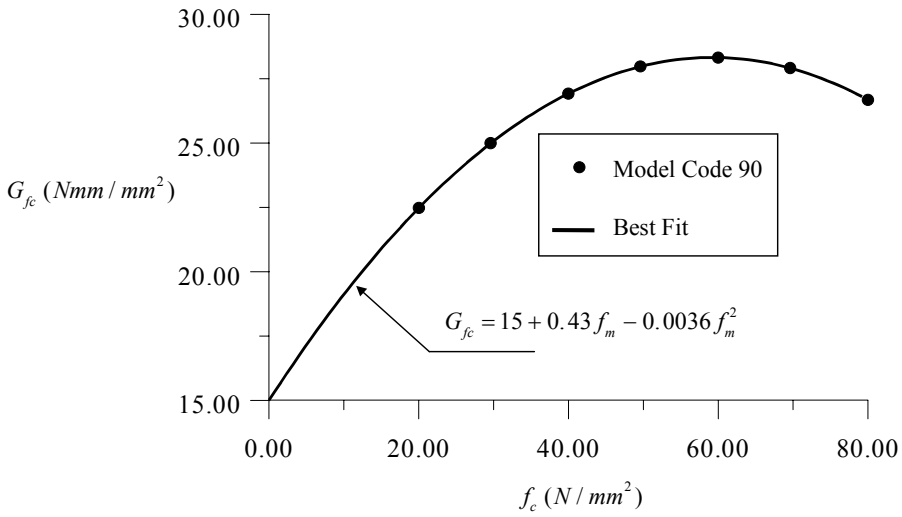

Figure A.2 – Compressive fracture energy according to the Model Code 90

Azurém, P – 4800-058 Guimarães Tel. +351 253 510200 • Fax +351 253 510217

With the hypotheses given above, the resulting elastic and non-linear material data are shown in *Table A.1*.

Table A.1 - Material properties for mortar series

Series	$f_{t,fl}$ *	$f_{c,cubes}$ *	f_{cm}	E	ν	f_{tm}	G_{fm}	G_{fcm}
1	-	13.0	10.4	21800	0.2	0.54	26	19
2	-	21.0	16.8	25600	0.2	1.29	36	21
3	9.2	56.3	45.0	35500	0.2	9.20	72	27
4	2.0	53.5	42.8	34900	0.2	2.00	69	27
5	1.4	28.3	22.6	28200	0.2	1.40	44	23
6	1.7	38.6	30.9	31300	0.2	1.70	55	25
-	N/mm^2	N/mm^2	N/mm^2	N/mm^2	-	N/mm^2	N/m	N/mm

* Experimental values, Sarralbo (2002)

A.2 Mechanical properties for Layer 1 - Mortar

According to Sarralbo (2002), different mortar types have been used for the masonry shells, see *Table A.2* for the properties of Layer 1.

Table A.2 - Material properties for mortar top layer in shell tests

Shell	Mortar	f_{cm}	E	ν	f_{tm}	G_{fm}	G_{fcm}
1 / 2	2	16.8	25600	0.2	1.29	36	21
3	3	45.0	35500	0.2	9.20	72	27
4	4	42.8	34900	0.2	2.00	69	27
5	6	30.9	31300	0.2	1.70	55	25
-	-	N/mm^2	N/mm^2	-	N/mm^2	N/m	N/mm

Azurém, P – 4800-058 Guimarães Tel. +351 253 510200 • Fax +351 253 510217

A.3 Mechanical properties for Layer 2 - Masonry

Masonry is an orthotropic material due to the geometry and anisotropy of the bricks. To represent the constitutive behavior of masonry the model detailed in Chapter 3 will be adopted. The available experimental results are:

- The compressive strength of the brick along the x direction f_{bx} is equal to 49.2 N/mm^2, Sarralbo (2002);
- The net compressive strength of the brick along the y direction $f_{bx,\,net}$ is 60% of the net compressive strength along the x direction due to the extrusion process, Oliveira et al. (2002). The percentage of holes in the x direction is 22%, the equivalent area in the y direction is 280 mm and the apparent area in the y direction is 450 mm. Therefore, the compressive strength of the brick along the y direction f_{by} is equal to $49.2 / (1 - 0.22) \times 280 / 450 = 39.2$ N/mm^2;
- The net tensile strength of the brick along the x direction is 3.82 MPa, Lourenço et al. (2002), resulting in a tensile strength along the x direction f_{btx} equal to $3.82 \times (1 - 0.22) = 3.0$ N/mm^2;
- The net tensile strength of the brick along the y direction is 2.75 MPa, Lourenço et al. (2002), resulting in a tensile strength along the y direction f_{bty} equal to $2.75 \times 280 / 450 = 1.7$ N/mm^2;
- The net bond strength of the mortar will be assumed as the minimum of the values indicated in Lourenço et al. (2002), $f_{t,\,bond}$ = 1.93 Mpa, divided by a factor two, associated with bond deterioration due to moisture transfer, see van der Pluijm (1999). Taking into account the actual area of the bricks, the following values are obtained along the material axes $f_{tx,\,bond} = 1.93 / 2 \times (1 - 0.22) = 0.75$ N/mm^2 and $f_{ty,\,bond} = 1.93$ N/mm^2;
- The fracture energy $G_{f,\,bond}$ found in Lourenço et al. (2002) was 8 N/m. Similar reasoning to the above for the fracture energy along the material axes results in $G_{fx,\,bond} = 8 / 2 \times (1 - 0.22) = 3.1$ N/m and $G_{fy,\,bond} = 8 / 2 = 4.0$ N/m;
- The cohesion of the joints c is equal to 1.39 N/mm^2, Oliveira et al. (2002);

The material data required for advanced non-linear calculations will be estimated taking into account the above experimental data and the geometry of masonry constituents, as:

Azurém, P – 4800-058 Guimarães Tel. +351 253 510200 • Fax +351 253 510217

- The Young modulus of masonry E has been estimated from inverse fitting of the experimental results, and reads E = 14000 N/mm^2. The Poisson coefficient of masonry ν is assumed equal to 0.2;
- The compressive strength of masonry f_m depends on the compressive strength of the unit and of the mortar, being given by $f_m = 0.60 \times f_b^{0.65} \times f_{cm}^{0.25}$, see Eurocode 6. From this formula, the values of *Table A.3* are found;
- The fracture energy in compression G_{fc} is given by the formula given in the previous section;
- The tensile strength along the x direction f_{tx} is given by a full crack crossing the joints $f_{tx} = (f_{tx,\,bond} \times 240 + f_{tm} \times 25) / 265$;
- The tensile strength along the y direction f_{ty} is given by a full crack crossing the joints $f_{ty} = (f_{ty,\,bond} \times 100 + f_{tm} \times 25) / 125$;
- The fracture energies are given similarly to the above as $G_{fx} = (G_{fx,\,bond} \times 240 + G_{fm} \times 25) / 265$ and $G_{fy} = (G_{fy,\,bond} \times 100 + G_{fm} \times 25) / 125$, respectively along the x and y directions;
- The additional parameters required for the orthotropic models are α = 1.0, β = –1.0 and γ = 3.0, see Lourenço (1996).

Table A.3 - Strength properties for masonry layer

Shell	Mortar	f_{cm}	f_{mx}	f_{my}	G_{fcx}	G_{fcy}	f_{tx}	f_{ty}	G_{fx}	G_{fy}
1 / 2	1	10.4	13.6	11.7	20	20	0.74	0.88	5.3	8.3
3	3	45.0	19.6	16.9	22	21	0.90	2.61	9.8	17.5
4	4	42.8	19.3	16.7	22	21	0.88	1.17	9.5	17.0
5	5	22.6	16.5	14.2	21	20	0.83	1.05	7.1	12.1
	-	*N/mm^2*	*N/mm^2*	*N/mm^2*	*N/mm*	*N/mm*	*N/mm^2*	*N/mm^2*	*N/m*	*N/m*

Azurém, P – 4800-058 Guimarães Tel. +351 253 510200 • Fax +351 253 510217

A.4 Mechanical properties for the steel

The Young modulus of steel E_s has been assumed equal 200000 N/mm^2 and the Poisson coefficient has been assumed equal to 0.2.

The stress-strain diagram for the different steel rebars used in the tests has not been characterized. It is well known that the steel strength is normally much higher than the yield value given by the steel producer. However, due to the lack of information, the actual steel strength of the different rebars used in the tests were taken from the Steel Class, see *Table A.4*.

Table A.4 - Strength properties for steel

Series	ϕ	Class	f_y
1, 2	8	S500	500
3	8	S500	500
4, 5	6	S400	400
-	*mm*	-	*N/mm^2*

Azurém, P – 4800-058 Guimarães Tel. +351 253 510200 • Fax +351 253 510217